AN ANALYSIS OF THE INTERACTIONS BETWEEN *CRYPTOCOCCUS NEOFORMANS* AND MURINE PULMONARY PHAGOCYTE SUBSETS

By

ASHLEE HAWKINS

Bachelor of Science in Microbiology

Oklahoma State University

Stillwater, Oklahoma

2018

Submitted to the Faculty of the
Graduate College of the
Oklahoma State University
in partial fulfillment of
the requirements for
the Degree of
MASTER OF SCIENCE
May, 2021

AN ANALYSIS OF THE INTERACTIONS BETWEEN

CRYPTOCOCCUS NEOFORMANS AND MURINE

PULMONARY PHAGOCYTE SUBSETS

Thesis Approved:

Karen Wozniak Ph.D

Thesis Adviser

Erika Lutter Ph.D

Craig Miller DVM,Ph.D

Name: ASHLEE HAWKINS

Date of Degree: MAY, 2021

Title of Study: AN ANALYSIS OF THE INTERACTIONS BETWEEN *CRYPTOCOCCUS NEOFORMANS* AND MURINE PULMONARY PHAGOCYTE SUBSETS

Major Field: Microbiology

Abstract: With over 220,000 cases and 180,000 deaths annually, *Cryptococcus neoformans* is the most common cause of fungal meningitis and a leading cause of death in HIV/AIDS patients in Sub-Saharan Africa. *C. neoformans* can either be killed by innate airway phagocytes, or it can survive intracellularly. Pulmonary macrophage and dendritic cell (DC) subsets have been identified, and we hypothesize that each subset has different interactions with *C. neoformans*. For these studies, we purified murine pulmonary macrophage and DC subsets – alveolar macrophages, $Ly6C^-$ and $Ly6C^+$ monocyte-like macrophages, interstitial macrophages, $CD11b^+$ and $CD103^+$ DCs.With each subset, we examined cryptococcal association, fungicidal activity, intracellular fungal morphology, cytokine secretion and transcriptional profiling. Results showed that all subsets associate with *C. neoformans*, but only monocyte-like macrophages inhibited growth. In addition, we observed sex differences in antifungal activity - the male $Ly6C^+$ monocyte-like macrophages inhibited cryptococcal growth, while the female $Ly6C^-$ monocyte-like macrophages inhibited cryptococcal growth. In addition, cytokine analysis revealed that phagocyte polarization is not responsible for the differences in fungicidal activity observed. Imaging flow showed differing ratios of cryptococcal morphologies, c-shaped or budding, depending on phagocyte subset. RNA sequencing analysis revealed the up regulation and downregulation of many genes, including immunological pathways and pathways relating to relating to metabolic activity. Future studies gaining a more in-depth understanding on the functionality of individual genes and pathways specific to permissive and non-permissive pulmonary phagocytes will allow identification of key targets when developing therapeutic strategies to prevent cryptococcal meningitis.

TABLE OF CONTENTS

Chapter Page

LIST OF TABLES

Table Page

LIST OF FIGURES

Figure Page

CHAPTER I

BACKGROUND AND INTRODUCTION

1.1 Ecology

Cryptococcus neoformans is an encapsulated fungal pathogen which is a part of the phylum Basidiomycota (Arras et al., 2017). The phylum Basidiomycota is only one of four fungal phyla that contains organisms that have the ability to infect humans based upon four criteria: the ability to grow above or at 37°C, the ability to digest and absorb components of human tissues, the ability to infect internal tissues by circumventing host barriers as well as the ability to withstand the human immune system (reviewed in (Kohler, Hube, Puccia, Casadevall, & Perfect, 2017)). All 19 species within the *Cryptococcus* genus are characterized as encapsulated budding yeast (Mitchell & Perfect, 1995). *Cryptococcus* species are spherically shaped yeast and are divided into four different distinct serotypes based upon capsular epitopes and their agglutination with specific antisera (Ikeda, Shinoda, Fukazawa, & Kaufman, 1982): serotypes A, B, C, and D (Franzot, Fries, Cleare, & Casadevall, 1998; Mitchell & Perfect, 1995). These four serotypes are further subdivided into two species, *C. neoformans* and *C. gattii* (D'Souza et al., 2011; Kwon-Chung et al., 2017) that make up eight major molecular types: VNI (var. *grubii*, serotype A), VNII (var. *grubii*, serotype A), VNIII (serotype AD), VNIV (var. *neoformans*, serotype D), VGI, VGII, VGIII, and VGIV (var. *gattii*, serotypes B and C) (Meyer et al., 2003). *C. neoformans* is distributed worldwide and has been isolated from various

environmental sources and is strongly associated with pigeon excreta (D. Ellis & Pfeiffer, 1992; Kwon-Chung & Bennett, 1984). *C. gattii* has been isolated from hollows and decayed wood of over 50 species of trees (Lin, Lin, Ho, Chen, & Chung, 2020), with the most notable being its specific association with *Eucalyptus camaldulensis* (D. H. Ellis, 1987; D. H. Ellis & Pfeiffer, 1990; Kwon-Chung & Bennett, 1984). *C. gattii* was initially considered to be endemic to tropical and subtropical regions until emergence of this pathogen occurred on the west of Canada resulting in the Vancouver Island Outbreak (Lam et al., 2019). Since then, the pathogen has spread throughout surrounding areas of the Pacific Northwest of the United States resulting in an established endemic among healthy residents and travelers (Jamil et al., 2020).

1.2 Epidemiology and Disease Manifestation

1.2.1 Epidemiology

Although the induction of antiretroviral therapy in 2003 has resulted in the decrease in AIDS-related deaths, the prevalence of cryptococcal infection has relatively remained unchanged (Jarvis et al., 2009). *C. neoformans* has been responsible for causing 223,100 infections and 181,100 deaths per year worldwide (Rajasingham et al., 2017). *C. neoformans* is the most common cause of central nervous system infections in individuals with HIV/AIDS. (Limper, Adenis, Le, & Harrison, 2017). The incidence of cryptococcal infection is prevalent in areas with a high frequency of HIV/AIDS infections and within areas that have very limited access to healthcare. Of the prevalence rates the majority of causes occur in sub-Saharan Africa (Grahnert et al., 2014; Benjamin J. Park et al., 2009; Rajasingham et al., 2017).

1.2.2 Disease

C. neoformans infection is known to occur by the inhalation of environmental spores or the exposure to desiccated feces of various avian species (Johnston, Voelz, & May, 2016; Zaragoza, 2019). *C. neoformans* infection can range from a mild pulmonary infection known as cryptococcal pneumonia to a more severe clinical manifestation - cryptococcal meningitis or

meningoencephalitis which occurs in immune compromised individuals (Baddley et al., 2008; Chayakulkeeree & Perfect, 2006). After inhalation into the lungs, the fungal pathogen encounters various components of the human immune system If successful, once *C. neoformans* evades the immune system it has the ability to travel systemically, gain access across the blood brain barrier and invade the central nervous system (Feretzaki, Hardison, Wormley, & Heitman, 2014; B. J. Park et al., 2009; Zaragoza, 2019). Patients with cryptococcal pneumonia present signs and symptoms of clinical pneumonia or upper respiratory infection (as reviewed in (Fisher, Montrief, Ramzy, Koyfman, & Long, 2021)). The most severe manifestation of *C. neoformans*, as a result of its dissemination into the central nervous system, is cryptococcal meningitis. Symptoms of meningoencephalitis include headache, confusion, elevated intracranial pressure, and in some cases blindness and altered mental state (reviewed in (Sloan & Parris, 2014)).

1.2.3 Treatments

The best clinical outcomes to treating cryptococcal meningitis are achieved using induction treatment with amphotericin B in combination with flucytosine (Day et al., 2013; Hai et al., 2019; Molloy et al., 2018). Flucytosine is chemically altered into fluorouracil within the *C. neoformans* yeast cell and acts to inhibit DNA synthesis within the pathogen (Carrillo-Muñoz, Giusiano, Ezkurra, & Quindós, 2006; Odds, Brown, & Gow, 2003) Amphotericin B (AmB) binds to ergosterol, a component of the cell membrane; once bound, AmB results in a loss of cell membrane integrity by the induction of pore formation (Ghaffar, Orr, & Webb, 2019; Peng et al., 2018). Although the use of AmB is effective, ergosterol is similar in structure to mammalian cholesterol and its toxicity toward mammalian erythrocytes and adverse side effects including nephrotoxicity and anemia are of great concern (Bicanic et al., 2015; Janout et al., 2015; Legrand, Romero, Cohen, & Bolard, 1992).

1.3 Mechanisms of Immune Evasion

1.3.1 Capsule

C. neoformans is surrounded by a thick polysaccharide capsule comprised of two major polysaccharides: glucuronoxylomannan (GXM) and galactoxylomannan (GalXM) (Cherniak, Jones, & Reiss, 1988; Heiss, Klutts, Wang, Doering, & Azadi, 2009; Zaragoza, 2019). The capsule surrounding *C. neoformans* plays a key role in the pathogen's virulence; studies show when the capsule is absent, virulence greatly decreases (Chang & Kwon-Chung, 1994; Zaragoza, 2019). The presence of the polysaccharide capsule has been shown to inhibit host cell phagocytosis (Bojarczuk et al., 2016; Kozel & Gotschlich, 1982; Kozel & Mastroianni, 1976; Macura, Zhang, & Casadevall, 2007). Most host cell macrophage cell surface receptor ligands reside within the cell wall of pathogens; *C. neoformans* thick polysaccharide capsule can mask the presence of these cell wall ligands from innate immune cells within the host (Zaragoza, 2019). The *C. neoformans* capsular component GXM induces effects that inhibit antigen presenting cell (APC) function (Vecchiarelli, Pietrella, Bistoni, Kozel, & Casadevall, 2002), causes the dysregulation of pro-inflammatory and anti-inflammatory cytokine secretion (Lopes et al., 2019; Monari et al., 2005), and increases the upregulation of FasL resulting in T Cell apoptosis (Piccioni et al., 2011). GalXM, like GXM, induces mirroring immunomodulatory effects such the induction of IL-6 in monocytes (Decote-Ricardo et al., 2019), the upregulation of TNF-α in peripheral blood mononuclear cells (PBMC) (Chaka et al., 1997), and the induction of T cell apoptosis at a rate ~50 times greater than GXM via the activation of caspase 8 (Pericolini et al., 2006).

1.3.2 Phagosome Manipulation

The intracellular nature of *C. neoformans* allows the fungal pathogen to reside and replicate within the macrophage lysosome (De Leon-Rodriguez, Rossi, Fu, Dragotakes, Coelho, Guerrero Ros, et al., 2018; Stuart M. Levitz et al., 1999). The polysaccharide capsule of *C. neoformans* and

the pathogen's ability to produce melanin allows for protection against the reactive oxidative species within the lysosome (Cox et al., 2003; Wang, Aisen, & Casadevall, 1995; Zaragoza et al., 2008). In addition, it has been shown that *C. neoformans* can delay phagolysosome maturation by interfering with the acquisition of critical phagosome maturation markers consisting of Rab GTPases and blocking acidification of the phagosome (Smith, Dixon, & May, 2015).

1.4 Murine Pulmonary Macrophages with *Cryptococcus neoformans*

Innate immune cells serve as the first line of defense against invading airway pathogens (Cheung, Halsey, & Speert, 2000; De Leon-Rodriguez, Rossi, Fu, Dragotakes, Coelho, Ros, et al., 2018; Espinosa & Rivera, 2016; Lloyd & Marsland, 2017; Margalit & Kavanagh, 2015). It is recognized that macrophages residing within tissue, tissue resident macrophages, are derived from diverse progenitors, including embryonic origins and terminally differentiated circulating monocytes (Epelman, Lavine, & Randolph, 2014; C. Zhang, Yang, & Ericsson, 2021). In the mouse lung, macrophages are recruited to the lung tissue during a cryptococcal infection (Wozniak et al., 2009; Wozniak, Vyas, & Levitz, 2006). Over the years, many studies have examined the role of murine pulmonary macrophages in response to *Cryptococcus* (S. Arora, Olszewski, MA, Tsang, TM, McDonald, RA, Toews, GB, Huffnagle, GB, 2011; Chen et al., 2016; Feldmesser, Kress, Novikoff, & Casadevall, 2000; Hardison et al., 2010; Kawakami et al., 1994; Kechichian, Shea, & Del Poeta, 2007; C.M. Leopold Wager, 2014; C. M. Leopold Wager, 2015; Osterholzer, Chen, et al., 2009; Stepanova et al., 2018). Depending on the strain of mouse used for the model, the infecting strain of *Cryptococcus*, and even the inoculum used, different laboratories have drawn different conclusions.

C. neoformans can be a facultative intracellular pathogen *in vitro*, and *in vivo* it can sometimes be found intracellularly inside of macrophages in infected tissues (Hardison et al., 2010), or alternatively, macrophages can kill *C. neoformans* (De Leon-Rodriguez, Rossi, Fu, Dragotakes, Coelho, Ros, et al., 2018; Feldmesser et al., 2000; S. M. Levitz et al., 1999). Therefore,

macrophages are a major determinant of the outcome of a cryptococcal infection (Alanio, Desnos-Ollivier, & Dromer, 2011; Johnston et al., 2016; Kechichian et al., 2007; C. M. Leopold Wager, 2015; Mansour, Vyas, & Levitz, 2011; Sabiiti et al., 2014; Shao et al., 2005; Tenor, Oehlers, Yang, Tobin, & Perfect, 2015). In immunocompromised individuals, uncontrolled fungal pneumonia is followed by lethal dissemination to the CNS (Baddley et al., 2008; Olszewski, Zhang, & Huffnagle, 2010; B. J. Park et al., 2009). The ability of macrophages to contain a *Cryptococcus* infection is dependent upon the specific type of macrophage activation (S. Arora et al., 2005; Davis et al., 2013; Hardison et al., 2010; Muller et al., 2007; Osterholzer, Chen, et al., 2009; Osterholzer et al., 2011; Voelz, Lammas, & May, 2009; Y. Zhang et al., 2009).

During murine infections, macrophage-cryptococcal outcomes are dependent upon M1/M2 (classical/alternative) macrophage polarization pathways (reviewed in (C. M. Leopold Wager & Wormley, 2014)); however, macrophage polarization status is constantly in flux and influenced by cytokines in the microenvironment (Davis et al., 2013). Classically activated macrophages (M1) are induced by IFN-γ and are associated with reduced fungal burden, enhanced fungicidal activity and the resolution of lung tissue inflammation. This is opposed to their alternatively activated (M2) counterparts (Davis et al., 2013; Hardison et al., 2010; C.M. Leopold Wager, 2014; C. M. Leopold Wager, 2015), which are associated with being a reservoir for replicating cryptococci (Hardison et al., 2010; Muller et al., 2007). STAT1 dependent activation pathways are essential for M1 polarization as well as for *C. neoformans* fungicidal activity via the production of nitric oxide (Hardison et al., 2012; Hardison et al., 2010; C.M. Leopold Wager, 2014; C. M. Leopold Wager, 2015). Infection of STAT1 KO mice and STAT1 conditional KO mice using an IFN-γ producing strain of *C. neoformans* resulted in increased fungal burden, increased M2 activation, and reduced anti-cryptococcal activity compared to WT mice (Hardison et al., 2012; C.M. Leopold Wager, 2014; C. M. Leopold Wager, 2015; C. M. Leopold Wager et al., 2018).

Classically activated macrophages produce large amounts of nitric oxide, a main effector mechanism contributing to anti-cryptococcal activity (Hardison et al., 2012; Hardison et al., 2010; C.M. Leopold Wager, 2014; C. M. Leopold Wager, 2015; Y. Zhang et al., 2010; Y. Zhang et al., 2009). Pulmonary macrophages isolated from mice deficient in iNOS, an enzyme necessary for nitric oxide production, display increased intracellular cryptococcal replication (C. M. Leopold Wager, 2015). In the murine lung environment, response to a *C. neoformans* infection results in a fluctuating Th1/Th2 T cell cytokine response over time (S. Arora, Olszewski, MA, Tsang, TM, McDonald, RA, Toews, GB, Huffnagle, GB, 2011). A higher IL-4/IFN-γ ratio contributes to a greater polarization towards the M2 phenotype, whereas a lower IL-4/IFN-γ ratio contributes to a greater polarization towards the M1 phenotype. Equal amounts of IL-4/IFN-γ lead to an M1/M2 intermediate macrophage phenotype that may support chronic "steady-state" fungal infections (S. Arora, Olszewski, MA, Tsang, TM, McDonald, RA, Toews, GB, Huffnagle, GB, 2011). Intracellular cryptococcal replication in murine alveolar macrophages induces phagolysosome damage. However, once the cells are polarized to the M1 phenotype via stimulation with IFN-γ, the macrophages can successfully kill *C. neoformans*, and the ability for the pathogen to induce phagolysosome damage is abolished (Davis et al., 2015). While these findings relate to macrophage activation status, the initial interactions between lung macrophages (prior to activation to either the M1 or M2 phenotype) with *Cryptococcus* are currently unknown. This may be due to the presence of multiple macrophage subsets present in the lung (Vermaelen & Pauwels, 2004) (Gautier et al., 2012; Gibbings et al., 2017; Misharin, Morales-Nebreda, Mutlu, Budinger, & Perlman, 2013; Tan & Krasnow, 2016; Zaynagetdinov et al., 2013) and our lack of knowledge in understanding the role(s) of each subset with *C. neoformans*.

1.5 Murine Pulmonary Macrophage Populations

The murine pulmonary cavity consists of a heterogeneous population of macrophages which were identified by flow cytometry and gene expression profiling (Gautier et al., 2012; Gibbings et al.,

2017; Misharin et al., 2013; Tan & Krasnow, 2016; Vermaelen & Pauwels, 2004; Zaynagetdinov et al., 2013). The distinct populations were identified as: alveolar macrophages, interstitial macrophages, monocyte-like Ly6C^{+} macrophages and monocyte-like Ly6C^{-} macrophages, each expressing unique cell surface markers (Misharin et al., 2013; Zaynagetdinov et al., 2013) as shown in table 1. Alveolar macrophages are defined as CD11c^{+}, CD11b^{-}, F4/80^{+}, SiglecF^{hi}, CD68^{hi}, and interstitial macrophages are F4/80^{+}, CD11b^{+}, Cd11c^{lo}, Gr1^{-}, and MHC II^{+}. Monocyte-like Ly6C^{-} macrophages are F4/80^{+}, CD11b^{+}, Cd11c^{-}, Gr1^{lo}, CD14^{+}, MHC II^{-}, and Ly6C^{-}, while the monocyte-like Ly6C^{+} macrophages have the same markers but are Ly6C^{+} (Guilliams et al., 2013; Manfred Kopf, Schneider, & Nobs, 2014; Misharin et al., 2013; Zaynagetdinov et al., 2013). Although each population has not been extensively studied with *C. neoformans*, murine alveolar macrophages and interstitial macrophages have been examined.

Table 1. Markers for murine pulmonary macrophage and dendritic cell subsets.

Marker	Alveolar Macrophage	Interstitial Macrophage	Ly6c+ Monocyte-like Macrophage	Ly6c- Monocyte-like Macrophage	CD103^{+} Dendritic Cell	CD11b^{+} Dendritic Cell
CD45	+	+	+	+	+	+
CD11b	-	+	+	+	-	+
CD11c	+	lo	+/-	+/-	+	+
CD68	hi	lo	-	-	hi	hi
MHC II	+/-	+	-	-	+	+
Siglec F	hi	-	-	-	-	-
F4/80	+	+	+	+	-	-
CD14	-	lo			-	-
CD24	-	-	-	-	+	+
CD103	-	-	-	-	+	-
Ly6c	-	-	+	-	-	-
Ly6G	-	-			-	-
CD115	-	-	-	-	-	-
CCR2	-	-	+	+	-	-/+

Murine pulmonary macrophages/monocytes are divided into 4 subsets and pulmonary conventional DCs are divided into 2 subsets based on cell surface expression of multiple markers. Symbols within table are defined as the following: hi = high expression, lo = low expression, + = positive, - = negative, +/- = intermediate expression. (Gibbings et al., 2017; Guilliams et al., 2013; Hey, Tan, & O'Neill, 2016; M. Kopf, Schneider, & Nobs, 2015; Menezes et al., 2016; Misharin et al., 2013; Nelson, Hawkins, & Wozniak, 2020; Yang, Zhang, Yu, Yang, & Wang, 2014; Zaynagetdinov et al., 2013).

1.5.1 Murine Alveolar Macrophages

Murine alveolar macrophages are the first line of defense against inhaled pulmonary pathogens (Todd et al., 2016; Xu & Shinohara, 2017). Alveolar macrophages are tissue resident macrophages of the alveoli that are derived during early fetal development from either the fetal yolk sac or fetal liver (reviewed in (Hoeffel et al., 2015; Manfred Kopf et al., 2014)). During early developmental stages, fetal monocytes colonize embryonic lungs, and upregulate surface expression of Siglec F and CD11c, and develop into tissue resident alveolar macrophages (Guilliams et al., 2013). After inhalation and phagocytosis of *C. neoformans,* alveolar macrophages showed intracellular replication of the fungus followed by macrophage cell lysis and the expulsion of live yeast cells into the extracellular space (Feldmesser et al., 2000). Alternatively, in some instances *C. neoformans* can replicate within macrophages and then escape via non-lytic expulsion or vomocytosis (Alvarez & Casadevall, 2007; Ma, Croudace, Lammas, & May, 2006). In mice lacking NK cells and T cells infected with a glucosylceramide deficient cryptococcal strain, Δ*gcs1,* depletion of alveolar macrophages by clodronate liposomes improved mouse survival and decreased the dissemination of *C. neoformans* to the central nervous system. This suggests that the alveolar macrophages were involved in the dissemination of *C. neoformans* (Kechichian et al., 2007). A more recent study examined murine alveolar macrophage polarization following infection with high- and low-uptake clinical *C. neoformans* isolates and

showed that the alveolar macrophages from mice infected with the high-uptake strains had increased expression of M2-associated genes (*Arg1, Fizz1, Il13 and Ccl17*), while those from mice infected with the low-uptake strains had increased expression of M1-associated genes (*Nos2, Ifng, Il6, Tnfa, Mcp1, Csf2, Ip10*) (Hansakon, Mutthakalin, Ngamskulrungroj, Chayakulkeeree, & Angkasekwinai, 2019), suggesting that cryptococcal strains may influence macrophage polarization.

1.5.2 Murine Interstitial Macrophages

Although few studies have examined murine interstitial macrophages, one study showed that interstitial macrophages harbored intracellular *C. neoformans* following intratracheal administration (Santangelo et al., 2004). In addition, the transfer of infected pulmonary interstitial macrophages, that were collected by agitating extracted lung tissue with sterile 5-mm diameter glass beads and morphologically characterized by Giemsa-stained smears and flow cytometry, into recipient mice via the tail vein led to hematogenous dissemination of *C. neoformans* to the brain (Santangelo et al., 2004).

1.5.3 Murine Inflammatory Monocytes

Murine inflammatory monocytes, $Ly6c^{+}$ and $Ly6c^{-}$ monocytes, are precursors to macrophages and DCs that are recruited to the site of infection, and these cells express the chemokine receptor CCR2 (reviewed in (Murray, 2018). In some studies, inflammatory monocytes seem to be important in cryptococcal clearance. Cryptococcal infection of $CCR2^{-/-}$ mice leads to Th2-type responses, increased lung fungal burden, and decreased recruitment of macrophages and DCs compared to WT mice (Osterholzer, Chen, et al., 2009; Osterholzer et al., 2011; Osterholzer et al., 2008; Traynor, Kuziel, Toews, & Huffnagle, 2000). In addition, in mice infected with *C. neoformans*, $Ly6C^{hi}$ $CCR2^{+}$ monocytes are recruited and can differentiate into fungicidal macrophages and DCs (Osterholzer et al., 2011; Osterholzer et al., 2008). Interestingly, a recent

study showed inflammatory monocytes are rapidly recruited to the lung during cryptococcal infection, but depletion of these cells leads to improved host survival, reduced pulmonary fungal burden, and reduced dissemination (Heung & Hohl, 2019). These cells also upregulate genes involved in M2 macrophage polarization, suggesting that in this model, the inflammatory monocytes differentiate into M2 macrophages, leading to a more severe outcome during cryptococcal infection (Heung & Hohl, 2019).

1.5.4 Murine pulmonary dendritic cells with *Cryptococcus neoformans*

Dendritic cells (DCs) play an important role in controlling *Cryptococcus* infections (reviewed in (Wozniak, 2018)). DCs are recruited to the murine lung during a cryptococcal infection (Wozniak et al., 2006), and in a protective model of cryptococcal infection, more DCs are recruited to the lungs in protected mice compared to non-protected mice, suggesting an anti-cryptococcal role for DCs (Wozniak et al., 2009). Following DC-cryptococcal interactions, DCs mediate the adaptive immune response by presentation of antigen to *Cryptococcus*-specific T cells (Wozniak et al., 2006). The depletion of pulmonary DCs, via the administration of diphtheria toxin (DT) to transgenic (Tg) mice, leads to increased morbidity and mortality as well increased B cell and neutrophil accumulation which causes severe lung inflammation (Osterholzer, Milam, et al., 2009).

1.5.5 Murine pulmonary dendritic cell populations

In the murine lung, DCs are a heterogeneous population consisting of distinct subsets characterized by extracellular and intracellular markers (Condon, Sawyer, Fenton, & Riches, 2011; Misharin et al., 2013; Shortman & Liu, 2002; Zaynagetdinov et al., 2013). This heterogeneous population consists of the $CD11b^+$ myeloid DCs, plasmacytoid DCs (pDCs) and $CD103^+$ DCs (Condon et al., 2011). $CD11b^+$ DCs are characterized by their high expression of CD11c, MHC class II, and absence of CD103. pDCs are characterized by expression of CD11c,

B220 and PDCA-1. Finally, $CD103^+$ DCs are characterized by their expression of CD103, CD11c, MHC class II and their lack of CD11b (Sung et al., 2006). Anatomically, the $CD103^+$ population localizes in the lung mucosa and along the lung vascular wall, however, few studies have examined these subsets in greater detail. $CD11b^+$ DCs are located mainly within the perivascular regions and are major producers of chemokines during homeostatic and inflammatory conditions of the lung (Beaty, Rose, & Sung, 2007; Furuhashi et al., 2012; Sung et al., 2006). Pulmonary plasmacytoid DCs (pDCs) infiltrate into the lungs during cryptococcal infection, and pDCs isolated from murine bone marrow have anti-cryptococcal activity (C. R. Hole et al., 2016). The recognition and uptake of *C. neoformans* by pDCs is dependent on expression of dectin-3 and the chemokine receptor CXCR3, and the fungicidal activity of pDCs is attributed to the production of reactive oxygen species (ROS) within the lysosome (C. R. Hole et al., 2016).

1.6 Objective and Aim of Study

Currently, there are no published data that provides an in-depth analysis of individual pulmonary phagocyte subsets and their initial interactions with *C. neoformans.* Thus, the overall objective of this study is to provide a detailed look into this interaction with an aim of determining if pulmonary phagocyte subsets interact differently with *C. neoformans* and to identify potential factors leading to said differences. Our central hypothesis is that murine pulmonary phagocyte subsets interact differently with *C. neoformans* resulting in either fungicidal activity or supporting an environment inducive to intracellular cryptococcal growth. In order to test our central hypothesis, we utilized a mouse model to isolate and purify six pulmonary phagocyte subsets and analyzed their interactions with *C. neoformans* ex vivo.

CHAPTER II

MATERIALS AND METHODS

2.1 Strains and media

C. neoformans strains H99 (Serotype A, mating type α) and mCherry producing strain KN99mCH (serotype A, KN99 mating type α), a kind gift from Dr. Jennifer Lodge (Washington University, St. Louis, MO), were recovered from 15% glycerol stocks, stored at -80°C prior to use in this study. Strains were maintained on yeast peptone dextrose (YPD) media agar plates. Yeast cells were grown for 18h at 30°C while shaking in YPD broth and collected by centrifugation, After the cells were washed three times with sterile phosphate-buffered saline (PBS), and viable yeast quantified using trypan blue dye exclusion on a hemocytometer before being diluted to the appropriate concentration for each particular assay.

2.2 Mice

Male and female BALB/c mice, approximately 5-6 weeks of age (Charles River Laboratories, Wilmington, MA) were used throughout these studies and were housed at Oklahoma State University Animal Resources. All studies were approved by Oklahoma State University's Institutional Animal Care and Use Committee (IACUC) and mice were handled according to IACUC guidelines.

2.3 Collection of murine pulmonary cells and tissue

2.3.1 Alveolar Macrophage Collection

Prior to euthanasia, mice were intravenously injected with anti-CD45 FITC (25ug/mL) (BD Biosciences, Franklin Lakes, NJ) diluted in PBS without calcium and magnesium 4-5 minutes prior to sacrifice in order to tag intravascular leukocytes within systemic circulation and separate these from pulmonary extravascular mononuclear phagocytes (Gibbings & Jakubzick, 2018). Mice were then euthanized via CO_2 inhalation followed by cervical dislocation. After euthanizing, the mouse trachea was exposed by making a vertical midline incision. A sterile 18-gauge cannula was inserted horizontally within the trachea with an attached syringe containing 1 ml sterile ice-cold PBS + 0.5% EDTA. The lungs were then lavaged three times with this solution to collect the bronchoalveolar lavage fluid (BAL), which was pooled into a sterile tube kept on ice.

2.3.2 Tissue macrophage and dendritic cell collection

For collection of lung tissue macrophages and dendritic cells, following collection of BAL, lungs were removed using aseptic technique, minced, and placed into digestion buffer (RPMI with 0.1mg/ml collagenase type IV (Sigma-Aldrich, St. Louis, MO). Tissues were enzymatically digested at 37°C for 30 min in 10 ml of digestion buffer. Following incubation, the digested tissues were then successively filtered through sterile 70- and 40-μm nylon filters (BD Biosciences) to enrich for leukocytes, and then cells were washed with sterile Hank's Balanced Salt Solution (HBSS). Erythrocytes were lysed by incubation in RBC lysis buffer (eBioscience, San Diego, CA) for 3 min on ice followed by a 2-fold excess of PBS.

2.4 Purification of Pulmonary Macrophage and Dendritic Cell Subsets

Alveolar macrophages were purified from a single cell suspension of BAL. Cells were enriched for alveolar macrophages first by blocking Fc receptors using purified rat anti-mouse CD16/CD32 (Mouse BD Fc block) (BD Biosciences) followed by positive selection using anti-

CD11c microbeads according to manufacturer's instructions (Miltenyi Biotec, Auburn, CA). Purity was verified using Labeling Check Reagent conjugated to VioBlue (Miltenyi Biotec) and CD11c and F4/80 fluorescently labeled antibodies by flow cytometry flow cytometry using an Acea Novocyte flow cytometer (Agilent Technologies, Santa Clara, CA), and purity above 95% was routinely achieved.

For purification of pulmonary tissue macrophages (interstitial macrophages, $Ly6C^+$ monocyte-like macrophages, and $Ly6C^-$ monocyte-like macrophages) and tissue DCs ($CD11b^+$ and $CD103^+$), Fc receptors were first blocked using Fc block (BD Biosciences). Next, FITC-labeled $CD45^+$ cells from the vasculature were removed using anti-FITC microbeads (Miltenyi Biotec). Following the removal of these cells, remaining cells were first selected (positively or negatively) by incubation with anti-CD11c microbeads (Miltenyi Biotec). Cells positively selected with CD11c were saved for further DC separations, while cells negatively selected were next positively selected using anti-F4/80 microbeads (Miltenyi Biotec) to select for macrophage subsets. The macrophage populations were next incubated with anti-MHC II microbeads (Miltenyi Biotec) – those positively selected are interstitial macrophages, while those negatively selected were subjected to further incubation with biotinylated anti-Ly6c antibody (Invitrogen, Waltham, Massachusetts) followed by selection with anti-biotin microbeads (Miltenyi Biotec) to distinguish $Ly6c^+$ monocyte–like macrophages (positively selected) from $Ly6c^-$ monocyte-like macrophages (negatively selected). For DC purification, the $CD11c^+$ cells were then incubated with anti-F4/80 microbeads (Miltenyi Biotec) to remove any contaminating macrophages. The $CD11c^+$ $F4/80^-$ cells were then incubated with anti-CD11b microbeads (Miltenyi Biotec). Cells positively selected with CD11b were $CD11b^+$ dendritic cells. Negatively selected CD11b cells ($CD11c^+$ $CD11b^-$) were then incubated with biotinylated anti-CD103 antibody (BD Biosciences) followed by selection with anti-biotin microbeads (Miltenyi), and positively selected cells were $CD103^+$ dendritic cells. Cell purity of each population was verified by using Labeling Check

Reagent (Miltenyi Biotec), and cell surface markers for each subset and analyzed by flow cytometry using an Acea Novocyte flow cytometer (Acea Biosciences, San Diego, CA). The cell separation scheme is summarized in Figure 1.

2.5 Flow Cytometry

Following cell separation, murine macrophage and DC subsets were resuspended in FACS buffer (PBS supplemented with 2% FBS) (100ul/well) and incubated with CD16/CD32 (Mouse BD Fc Block) (BD Biosciences) to block non-specific binding. Then, samples were stained with labeling check reagent (Miltenyi Biotec), CD45-APC/APC-Vio770 (Biolegend), CD11c-PE-Cy7 (BD Biosciences), Siglec F-PerCP-efluor (BD Biosciences), CD11b-FITC (BD Biosciences), F4/80-PE (Miltenyi Biotec), Ly6c-APC (BioLegend), MHC II-Superbright 645 (Invitrogen), CD103-PerCP-efluor (BD Biosciences) CD24-APC (BioLegend) a viability dye (LIVE/DEAD Fixable yellow, Invitrogen). Following this, cells were incubated with antibodies for 30 minutes at 4°C then washed three times with FACS buffer and fixed with 2% formaldehyde. Samples were analyzed on an Acea Novocyte 3000 flow cytometer (Agilent Technologies), and data were analyzed using NovoExpress software (Agilent Technologies).

2.6 Cryptococcal inhibition assay

Each subset of pulmonary macrophages or DCs were separated (as described above), and $2x10^5$ cells/ml of each subset were incubated with 1µg/ml anti-GXM antibody (kind gift from Tom Kozel, University of Nevada Reno) and $1x10^4$ cells/ml of *C. neoformans* strain H99 (20:1 ratio) in 100 µl in triplicate wells for 24 hours at 37°C, 5% CO_2. After 24 hours, the samples were centrifuged, and supernatants were removed. Macrophages were lysed for 15 minutes at room temperature using 100 µl sterile water. Samples were then serially diluted and plated on YPD agar. Plates were incubated for 48 hours at 30°C, and cryptococcal CFU were quantified.

2.7 Cryptococcal association assay

Each subset of pulmonary macrophages or DCs were separated (as described above), and $2x10^5$ cells/ml of each phagocyte subset were incubated with 1µg/ml anti-GXM antibody (Tom Kozel, University of Nevada Reno) and $1x10^4$ cells/ml of *C. neoformans* strain KN99mCherry (20:1 ratio) in 100 µl in triplicate wells for 2 hours at 37°C, 5% CO_2. After 2 hours, the samples were stained for cell surface markers (as described in Flow Cytometry methods) and the percent association of each subset with fluorescent *C. neoformans* was calculated using an Acea Novocyte 3000 flow cytometer and Novoexpress software (Acea Biosciences).

2.8 Imagestream Imaging Flow Cytometry

Murine phagocyte subsets were isolated as described above and $2x10^5$ cells/ml of each phagocyte subset were incubated with 1µg/ml anti-GXM antibody (Tom Kozel, University of Nevada Reno) and $2x10^5$ cells/ml *C. neoformans* strain Kn99mCherry (1:1 ratio) in 100 µl in triplicate wells for 2 hours at 37°C, 5% CO_2. Cells were stained with the following fluorophores: CD45-FITC/PerCP (BD Biosciences), MHC II-Alexa Fluor 488 (BD Biosciences), F4/80-PE (Invitrogen), CD103-PE (Invitrogen), CD11b-PE (Invitrogen), Siglec F-PE (BD Biosciences), Ly6c-PerCP-Cy5.5 (Novus Biologicals), CD11c-PerCP-Cy5.5(BD Biosciences) for 30 min at 4°C. Cells were washed three times with FACS buffer, followed by fixation with 1% ultrapure paraformaldehyde diluted with FACS buffer. Cells were analyzed in the in the Flow and Image Cytometry Laboratory at The University of Health Sciences Center (OUHSC, Oklahoma City, OK) using the Amnis Imagestream Mark II (Luminex, Austin, TX). Using the Amnis IDEAS 6.2 software (Luminex), the internalization masking feature was used and cells were selected based upon the internalization of KN99mCherry. Of the cells selected, 100 cells were quantified and analyzed for cryptococcal intracellular morphologies consisting of condensed (c-shaped), live, budding and debris. After quantification, percent killing of all subsets were calculated by total cells out of 100 that contained condensed (c-shape) cryptococcal cells and cryptococcal debris multiplied by 100.

2.9 Murine Macrophage and Dendritic Cell Subset Cytokine Analysis

Each subset of pulmonary macrophages or DCs were separated (as described above), and $2x10^5$ cells/ml of each phagocyte subset were incubated with 1µg/ml anti-GXM antibody and $1x10^4$ cells/ml *C. neoformans* strain H99 (20:1 ratio) in 100 µl in triplicate wells for 2 hours at 37°C, 5% CO_2. Cell supernatants were collected, and protease inhibitor (Thermo Scientific) was added to supernatants. Treated supernatants were placed in tubes and stored at -80° C until analysis. Supernatants were assayed for mouse cytokines/chemokines according to manufacturer's instructions (Bio-Plex Pro Mouse Cytokine 23-plex) and samples were read on a BioRad BioPlex®-200 (Bio-Rad, Hercules, CA). Data were analyzed using GraphPad Prism v5.0 (GraphPad Software, San Diego, CA).

2.10 RNA Sequencing of Phagocyte Subsets Following Interaction with *C. neoformans*

Following incubation of each macrophage or DC subset with *C. neoformans* strain H99 at a ratio of 20:1 and 1µg/ml anti-GXM antibody at 37°C, 5% CO_2 for 2h, cells were collected and stored in Trizol (Invitrogen) at -20°C until analysis. RNA purification was conducted by Novogene (Novogene Corp, Sacramento, CA). Next, murine RNA-sequencing was conducted using SMARTer Stranded V2 library prep and samples were sequenced on the Illumina Platform (PE150 Q30≥80%) (Novogene Corp). Gene expression was compared between each macrophage and DC subset alone and when incubated with *C. neoformans* strain H99. Significant differences within gene expression were calculated using readcount adjusted by trimmed mean of M-values (TMM), then differential significant analysis was performed using the edgeR package (Bioconductor, Fred Hutchinson Cancer Research Center, Seattle, WA) within R Studio (Delaware Public Benefit Corporation (PBC), Boston, MA), with the significant criterion being both qvalue < 0.005 and |log2(FoldChange)| > 1. Genes with significantly different expression values were grouped into signaling pathways using KEGG Pathway Analysis and Ingenuity Pathway Analysis (IPA) software.

2.11 Statistical analysis

GraphPad Prism v5.0 (GraphPad Software, San Diego, CA) was used to detect significant differences between CFU of H99 alone compared to each test group within the cryptococcal inhibition assay by an unpaired two-tailed T test with a 95% confidence value with a p-value consisting of $p < 0.05$. An XY correlation analysis was used to determine correlation between CFU and percent interstitial macrophages. Differences in fungal/phagocyte association were tested using one-way ANOVA with Tukey's post-test, with significant differences defined as $p < 0.05$. IDEAS 6.2 software (Luminex Corporation, Austin, TX), was used to analyze and quantify intracellular cryptococcal morphologies out of a total of 100 phagocytes per subset. Significant differences in intracellular cryptococcal morphology and total cryptococcal killing was calculated with GraphPad Prism using an unpaired two-tailed T test with a 95% confidence value with a p-value consisting of $p < 0.05$. Significant differences within gene expression were calculated using sequencing readcount adjusted by the trimmed mean of M-values performed using the edgeR package (Bioconductor). Gene significance criterion was determined using both q-value <0.005 and $|\log2(\text{FoldChange})| > 1$. Genes with significantly different expression values were grouped into signaling pathways using KEGG Pathway Analysis. Cytokines were analyzed using Column Statistics with the use of GraphPad Prism. Significance was determined using an independent one sample t test with confidence interval 95% and p value: $p < 0.05$.

CHAPTER III

RESULTS

3.1 Murine pulmonary phagocyte subsets exhibit varying fungicidal activity

To evaluate the fungicidal activity of phagocyte subsets within the murine pulmonary cavity, subsets of pulmonary macrophages (alveolar, interstitial, $Ly6C^-$ monocyte-like and $Ly6C^+$ monocyte-like) and conventional DCs ($CD11b^+$ and $CD103^+$) were separated (Figure 1) and used in anti-cryptococcal assays. In preliminary studies using murine alveolar and pulmonary lung tissue macrophages, both alveolar macrophages and the lung tissue macrophage population displayed a difference in fungicidal activity. Statistical analysis revealed that there was a significant decrease ($p < 0.05$) in the amount of cryptococcal growth (CFU/ml) when analyzing the alveolar macrophage population as compared to the *C. neoformans* lab strain H99 growth control but there was no significant difference found when analyzing the lung tissue macrophage population (Figure 2a). The lung tissue phagocyte population exhibited a variable range of anti-cryptococcal activity which led to the further division of phagocyte subsets in subsequent experiments. Next, we proceeded to evaluate the monocyte-like macrophage populations as shown in Figure 2b. There was a significant decrease ($p < 0.05$) in the amount of cryptococcal growth (CFU/ml) when *C. neoformans* was incubated with the monocyte-like macrophages compared to the growth of *C. neoformans* strain H99 alone. In addition, there were no significant differences seen in both the alveolar macrophage population and the further division of the

interstitial macrophage population as compared to the H99 growth control, as shown in figure 2b,

Next, the monocyte-like macrophage population was further subdivided into two populations: $Ly6c^-$ and $Ly6c^+$ monocyte-like macrophages following the separation scheme as shown in Figure 1. The fungicidal activity of these two populations were assessed as shown in Figure 3a. Statistical analysis revealed that there was no significant difference in antifungal activity following incubation of *C. neoformans* with either $Ly6c^-$ or $Ly6c^+$ monocyte-like populations as compared to *C. neoformans* strain H99 alone. In addition, there were no significant differences found in both the alveolar macrophage population and the interstitial macrophages as compared to the H99 growth control. In order to eliminate sex as a biological variable, experiments were performed in both male and female mice. However, we noticed differences in these data, so the data were stratified by sex. Male $Ly6C^+$ monocyte-like macrophages showed a trend towards inhibiting the growth of *C. neoformans,* although this was not statistically different (p=0.28) (Figure 3b), while the female $Ly6C^-$ monocyte-like macrophages significantly inhibited cryptococcal growth (p=0.03) compared to *C. neoformans* grown in media alone (Figure 3c). These results demonstrate that murine pulmonary phagocyte subsets interact differently with *C. neoformans* and the sex of the host could determine disease severity. Next, we proceeded to evaluate the fungicidal activity of two pulmonary dendritic cell populations: $CD11b^+$ and $CD103^+$. As shown in Figure 4a, the dendritic cell (DC) populations were isolated and purified following a similar procedure as with the macrophage populations (Figure 1). When pulmonary DC subsets ($CD11b^+$ and $CD103^+$ DCs) were assayed for the fungicidal activity, there were no significant differences in cryptococcal growth following incubation with both $CD103^+$ and $CD11b^+$ DC subsets as compared to the *C. neoformans* strain H99 alone (Figure 4a). Within the two pulmonary dendritic cell sub-populations $CD11b^+$ and $CD103^+$, the male $CD11b^+$ population exhibited significant inhibition of cryptococcal growth (figure 4b), while the female dendritic cell populations did not exhibit any significant differences in cryptococcal growth as compared to *C.*

neoformans strain H99 (figure 4c). These results demonstrate that murine pulmonary phagocyte subsets interact differently with *C. neoformans* and the sex of the host could determine disease severity.

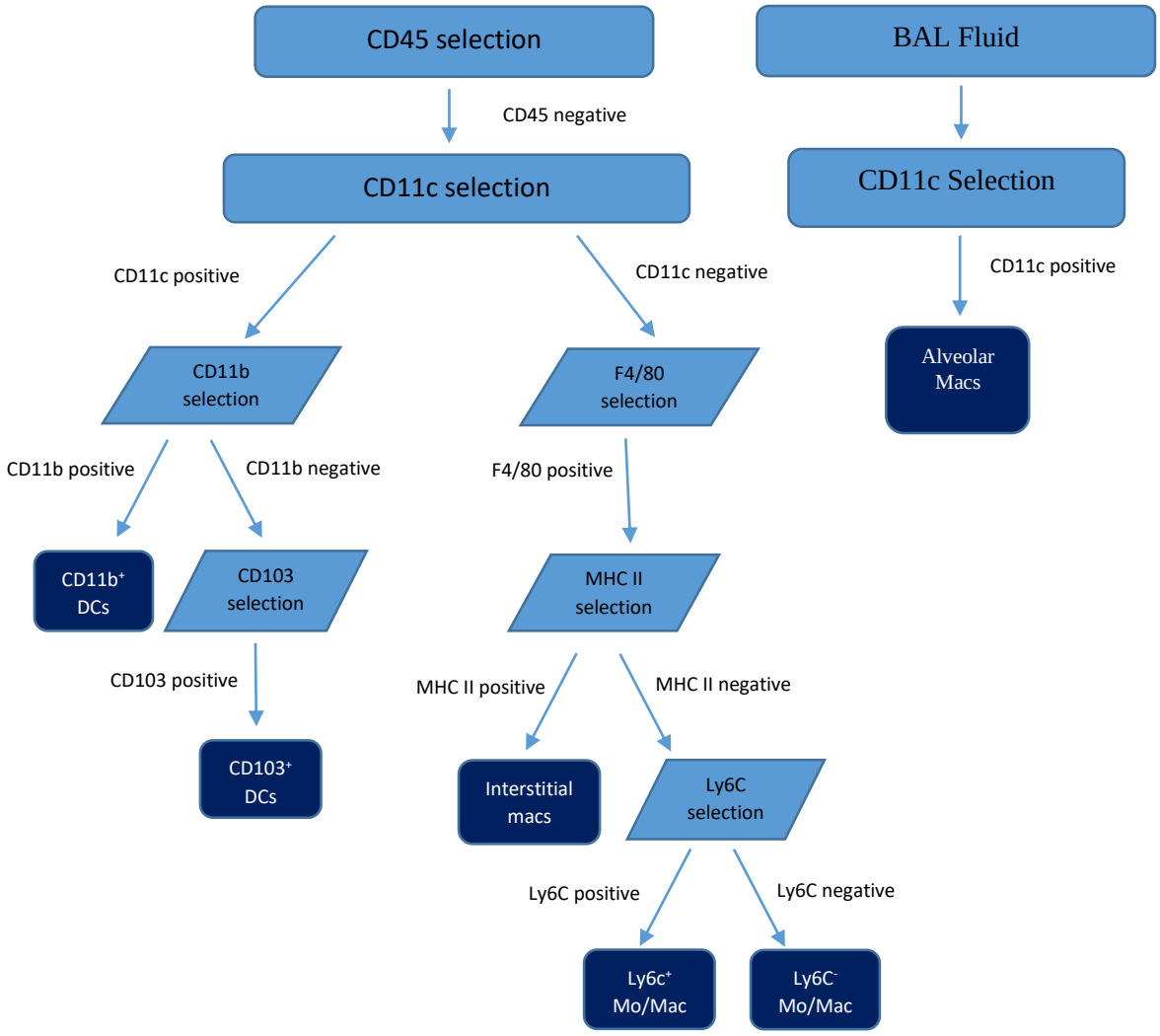

Figure 1. Purification of Murine Tissue Macrophage and Dendritic Cell Subsets

Following lung tissue collagenase digestion, labeled $CD45^{+}$cells from the circulation are removed, and tissue macrophage and dendritic cell subsets were separated using a series of magnetic separations. Lung tissue is pooled from 20 mice, collagenase digested, then separated into single-cell suspensions before magnetic separation. Cell purity is measured by flow cytometry post-separation.

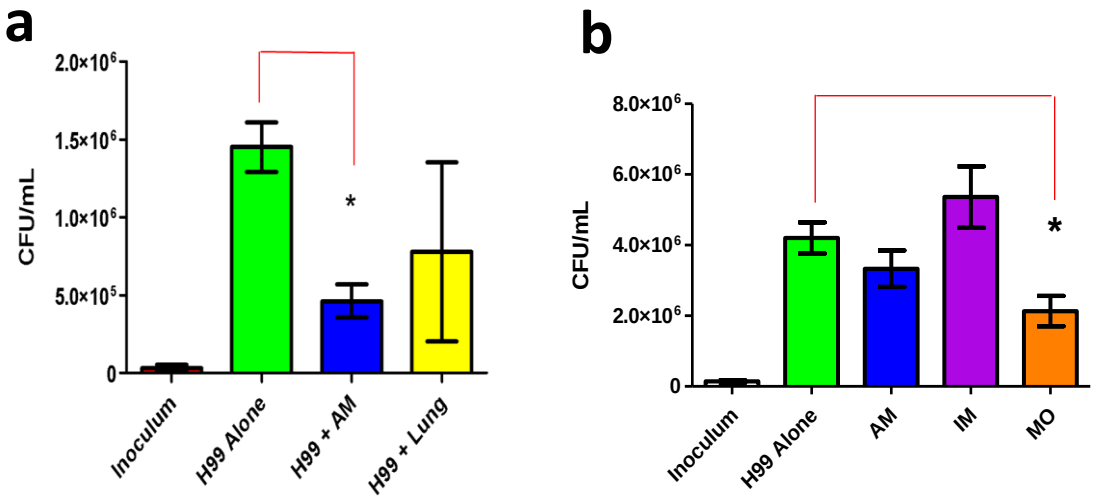

Figure 2. Murine pulmonary macrophage subsets interact differently with *C. neoformans*.

Murine pulmonary phagocyte subsets interact differently with *C. neoformans.* Pulmonary phagocytes were purified from BALB/c mice and incubated with C. neoformans strain H99 for 24hrs at a ratio of 20:1. Macrophages were lysed and plated on YPD agar and CFUs were counted. Graph (a) shows CFU counts in CFU/mL following *C. neoformans* strain H99 incubation alone (H00), with alveolar macrophages (AM) and with lung tissue phagocytes (Lung). Inoculum indicates initial *C. neoformans* strain H99 concentration prior to incubation. Graph (b) shows CFU counts in CFU/mL following *C. neoformans* strain H99 incubation alone (H99), with alveolar macrophages (AM), with interstitial macrophages (IM) and monocytes (MO). The data are means ± standard errors of the means (SEM) for three experiments each. A

two tailed unpaired t test was performed with each phagocyte population compared to cryptococcal growth of the *C. neoformans* H99 control group. Significant differences shown in graphs (b) and (c) represent *p-value <0 .05.

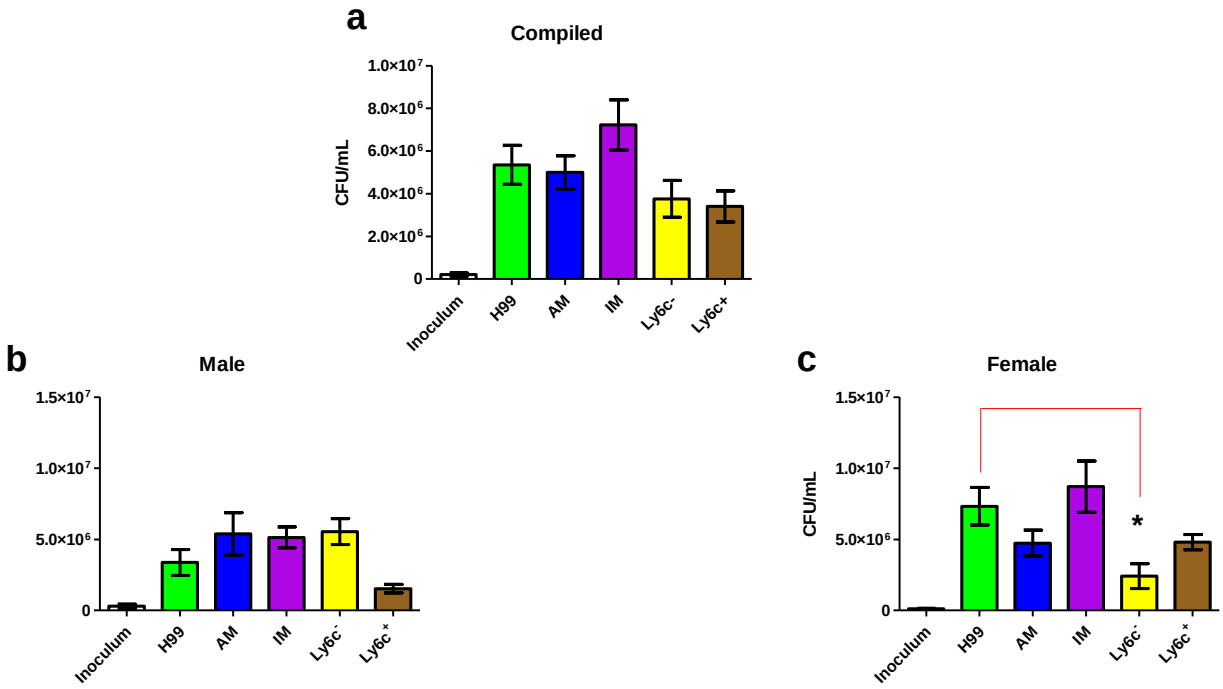

Figure 3. Murine pulmonary macrophage subsets exhibit differing anti-cryptococcal capabilities dependent upon sex. Pulmonary macrophage subsets were purified from both male and female BALB/c mice and incubated with *C. neoformans* strain H99 for 24hrs at 37°C, 5% CO_2 at a ratio of 20:1. Macrophages were lysed and plated on YPD agar and CFUs were counted. Graph (a) shows CFU counts in CFU/ml from both male and female phagocyte populations following *C. neoformans* strain H99 incubation alone (H99), with alveolar macrophages (AM), with interstitial macrophages (IM), with Ly6c$^-$ monocyte-like macrophages (Ly6c$^-$) and Ly6c$^+$ monocyte-like macrophages (Ly6c$^+$). Inoculum indicates initial *C. neoformans* strain H99 concentration prior to incubation. Graph (b) shows CFU counts in CFU/mL from male phagocyte

populations following incubation with *C. neoformans* strain H99. Graph (c) shows CFU counts in CFU/mL from female phagocyte populations following incubation with *C. neoformans* strain H99. The data are means ± standard errors of the means (SEM) for three independent experiments each of both male and female mice each done in triplicate. A two tailed unpaired t test was performed with each phagocyte population to compared to cryptococcal growth of the *C. neoformans* H99 control group. Significant differences (*) shown in graph (b) represent a $p < 0.05$.

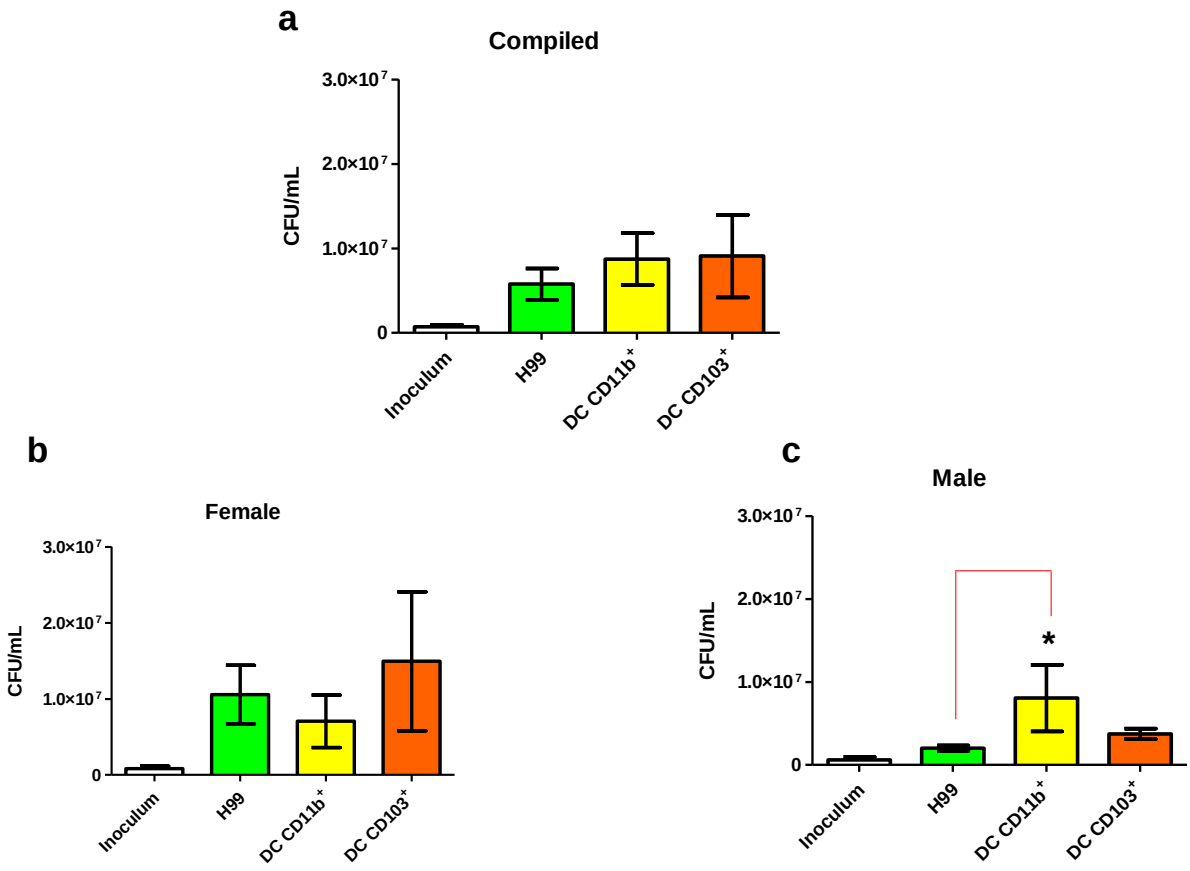

Figure 4. Murine pulmonary dendritic cell subsets exhibit differing anti-cryptococcal capabilities dependent upon sex. Pulmonary dendritic cell (DC) subsets were purified from both male and female BALB/c mice and incubated with *C. neoformans* strain H99 for 24hrs at 37°C,

5% CO_2 at a ratio of 20:1. DCs were lysed and plated on YPD agar and CFUs were counted. Graph (a) shows CFU counts in CFU/mL from both female and male dendritic cell populations following *C. neoformans* strain H99 incubation alone (H99), with $CD11b^+$ dendritic cells (DC $CD11b^+$), and $CD103^+$ dendritic cells (DC $CD103^+$). Inoculum indicates initial *C. neoformans* strain H99 concentration prior to incubation. Graph (b) shows CFU counts in CFU/ml from female dendritic cell populations following incubation with *C. neoformans* strain H99. Graph (c) shows CFU counts in CFU/ml from male dendritic cell populations following incubation with *C. neoformans* strain H99. The data are means ± standard errors of the means (SEM) for three independent experiments of each sex. A two tailed unpaired t test was performed with each DC population compared to cryptococcal growth of the *C. neoformans* H99 control group. Significant differences (*) shown in graph (b) represent a $p < 0$ .05.

3.2 Murine pulmonary phagocyte subsets interact with *C. neoformans*

In order to verify that *C. neoformans* interacted with murine pulmonary phagocyte subsets equally (and that any differences in antifungal activity were not attributable to differences in interaction), both male and female pulmonary macrophage and DC subsets were incubated with an m-cherry expressing *C. neoformans* strain (KN99mCH) for 2 hours at 37°C, 5% CO_2 at a ratio of 1:1. Following incubation, cells were stained and examined by flow cytometry. When analyzing macrophage subsets and *C. neoformans* association, data showed that all subsets interacted with *C. neoformans*, and there were no significant differences between the populations (Figure 5a), even when sexes were stratified (Figure 5b and 5c). When analyzing DC-*C. neoformans* association via flow cytometry, results showed that both DC subsets ($CD103^+$ and $CD11b^+$ DCs) interact with *C. neoformans* (Figure 6a), even when sexes were stratified (Figure 6b and 6c). These results show that all pulmonary phagocyte subsets have the ability to interact with *C. neoformans* ex vivo.

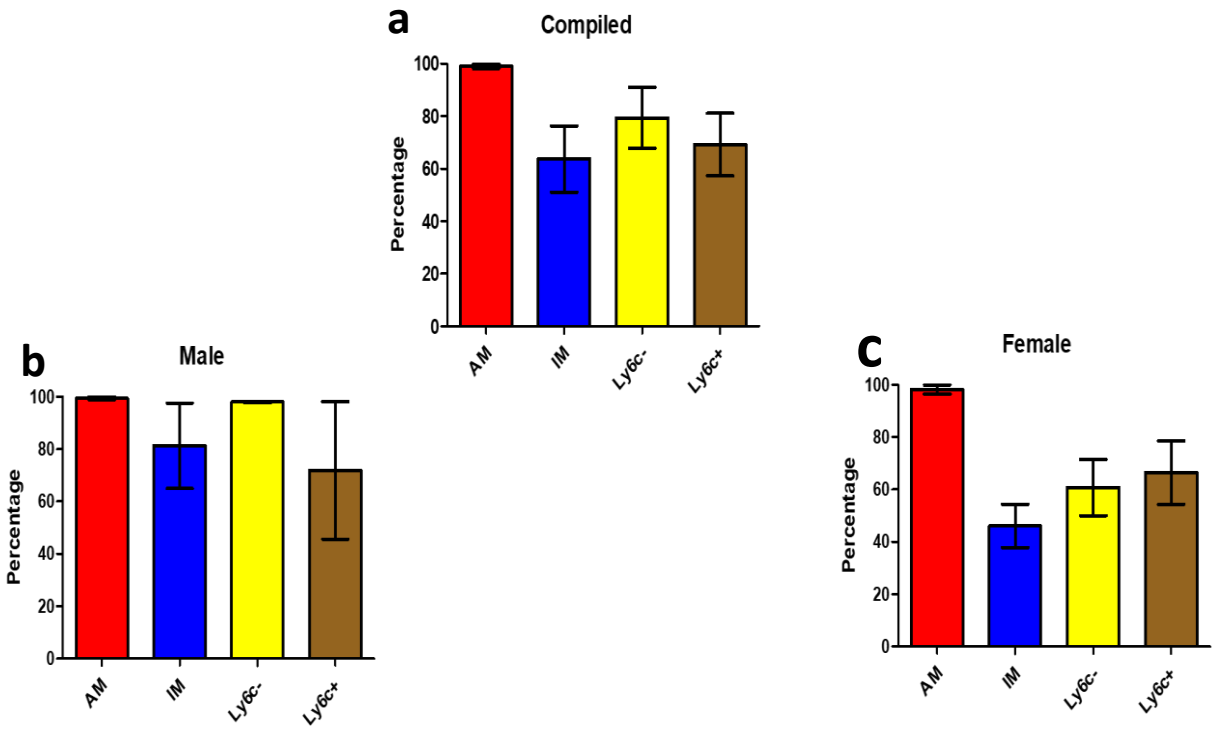

Figure 5. Murine pulmonary phagocyte subsets interact with *C. neoformans* ex vivo.

Pulmonary macrophage subsets were purified from both male and female BALB/c mice and incubated with m-cherry expressing *C. neoformans* (Kn99mCH) for 2hrs at 37°C, 5% CO_2 at a ratio of 1:1. Following incubation, cells were stained for surface markers and analyzed for cryptococcal association via flow cytometry. Graph (a) shows *C. neoformans* strain H99 association percentages (Percentage) for both male and female alveolar macrophage (AM), interstitial macrophage (IM), Ly6c$^-$ monocyte-like macrophages (Ly6c$^-$) and Ly6c$^+$ monocyte-like macrophages (Ly6c$^+$) phagocyte populations. Graph (b) shows *C. neoformans* strain H99 association percentages (Percentage) for male phagocyte populations. Graph (c) shows *C. neoformans* strain H99 association percentages (Percentage) for female phagocyte populations. The data are means ± standard errors of the means (SEM) for three independent experiments each of both male and female.

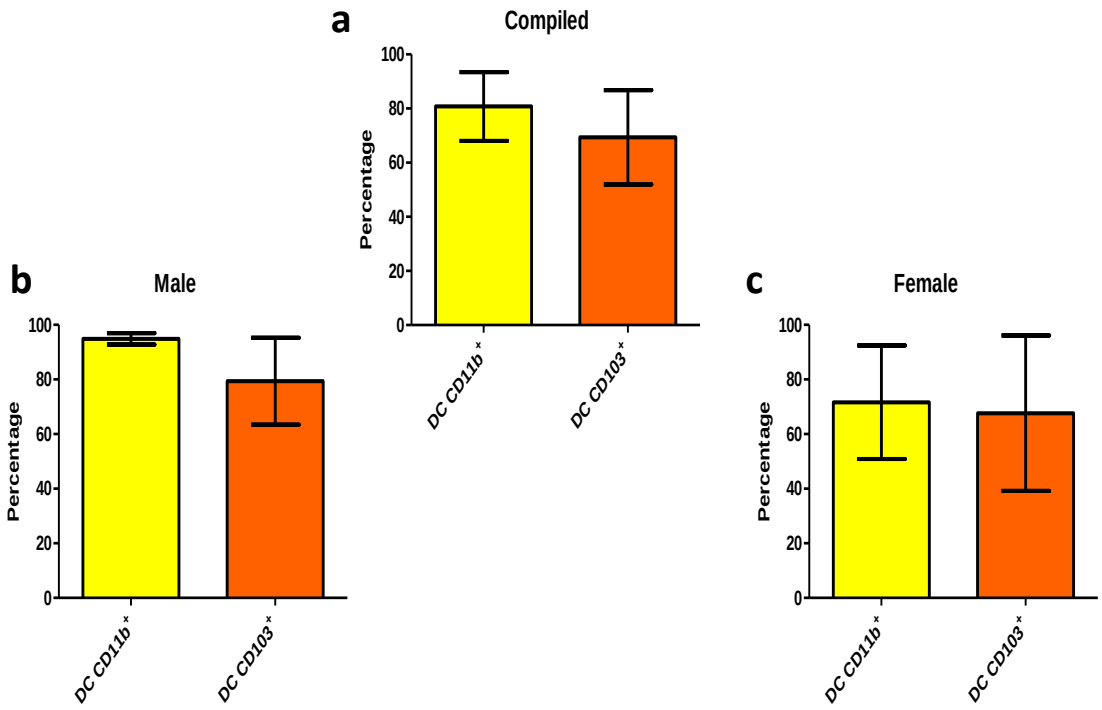

Figure 6. Murine pulmonary dendritic cell subsets interact with *C. neoformans* ex vivo. Pulmonary dendritic cells (DCs) were purified from both male and female BALB/c mice and incubated with m-cherry expressing *C. neoformans* (KN99mCH) for 2hrs at 37°C, 5% CO_2 at a ratio of 1:1. Following incubation, cells were stained for surface markers and analyzed for association via flow cytometry. Graph (a) shows *C. neoformans* strain H99 association percentages (Percentage) for both male and female $CD11b^+$ and $CD103^+$ dendritic cell populations. Graph (b) shows *C. neoformans* strain H99 association percentages (Percentage) for male dendritic cell populations. Graph (c) shows *C. neoformans* strain H99 association percentages (Percentage) for female dendritic cell populations. The data are means ± standard errors of the means (SEM) for three independent experiments each of both male and female.

3.3 Internalized *C. neoformans* display varying cryptococcal morphologies when interacting with pulmonary phagocyte subsets

In order to determine the cellular morphology of *C. neoformans* following the pulmonary phagocyte subset interaction, imaging flow cytometry was used. Both male and female pulmonary phagocyte subsets were incubated with an m-cherry expressing *C. neoformans* strain (KN99mCH) for 2 hours at 37°C, 5% CO_2 at ratio of 1:1. Following incubation, cells were purified and stained for $CD45^+$ leukocyte marker and cryptococcal morphologies were examined at a 40x magnification by the ImageStreamX-Imaging Flow Cytometer-MKII (Luminex). Figures 7a-7f and Figures 8a-8f show examples of intracellular cryptococcal morphologies of cryptococcal cells within both male and female phagocyte populations, respectively. Using IDEAS 6.2 software (Luminex), images were analyzed and varying cryptococcal morphologies were examined and quantified as described in Materials and Methods. Figure 7g and Figure 8g show a graphical representation of this quantitative analysis using GraphPad prism. Both male and female phagocyte subset populations contain varying intracellular cryptococcal morphologies and fungicidal activity as quantified in Figures 7g and 8g. Figure 7a-7f and Figure 8a-8f show distinct cryptococcal morphologies including circular, crescent-shaped (c-shaped), budding and debris. A circular and budding cryptococcal morphology is indicative of living and/or replicating cryptococcal yeast cells. The crescent-shaped morphology indicates dead and/or dying cryptococcal yeast cells. Structural changes in the cell membrane of live *C. neoformans* from circular to a crescent shaped morphology due to the rupturing of the cell wall is a possible indication of cryptococcal death (Camaron R. Hole, Bui, Wormley, & Wozniak, 2012). Data revealed female phagocyte sub-populations display varying intracellular cryptococcal morphologies upon uptake of the m-cherry-expressing *C. neoformans* strain (Figure 8a-8f). Quantitative analysis of the images from female phagocytes showed that $Ly6c^-$ monocyte-like macrophages were significantly better at killing *C. neoformans* than the $CD103^+$ DCs (Figure 8g).

In addition, there were significant differences in intracellular cryptococcal morphology (condensed and debris) when comparing the alveolar macrophages with both interstitial macrophages and CD103^{+} DCs. The CD103^{+} DCs showed significant differences intracellular cryptococcal morphology when compared to the following subsets – alveolar macrophages, interstitial macrophages, Ly6c^{-} monocyte-like macrophages, and CD11b^{+} DCs. (Figure 8g). There were no significant differences found when comparing the male intracellular cryptococcal morphologies and percentage of total fungicidal activity between subsets (Figure 7g).

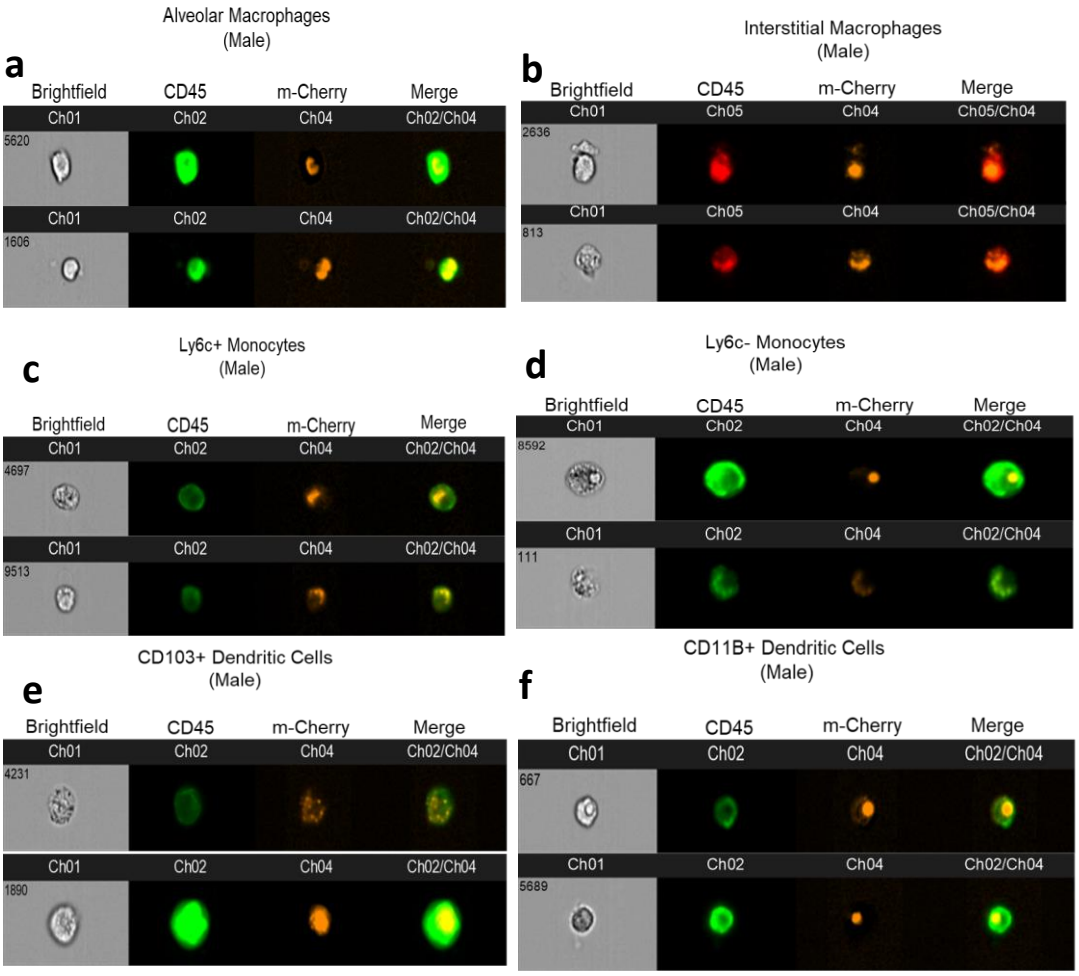

g

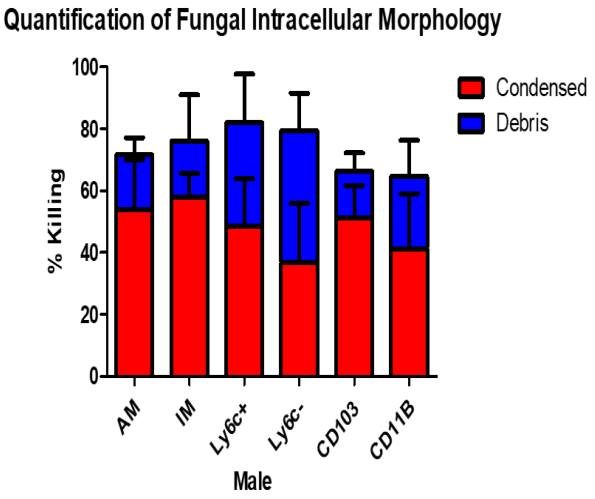

Figure 7. Murine pulmonary male phagocyte subsets display varying cryptococcal morphologies after *C. neformans* internalization. Using male BALB/c mice, phagocyte subsets were purified and incubated with m-cherry expressing *C. neoformans* (KN99Mch) for 2hrs at a ratio of 20:1. Following incubation, cells were stained for surface markers visualized at 40x magnification by the ImageStreamX-Imaging Flow Cytometer-MKII (Luminex). Figure 7a-7f display cryptococcal morphologies within each pulmonary phagocyte subset. Data of cryptoccocal morphology was quantified using IDEAS Software 6.2 and graphically expressed using GraphPad Prism (7g). The data are means ± standard errors of the means (SEM) for three independent experiments. One-way ANOVA with Tukey's post-test was used to detect significant differences (*) between groups, $p < 0.05$.

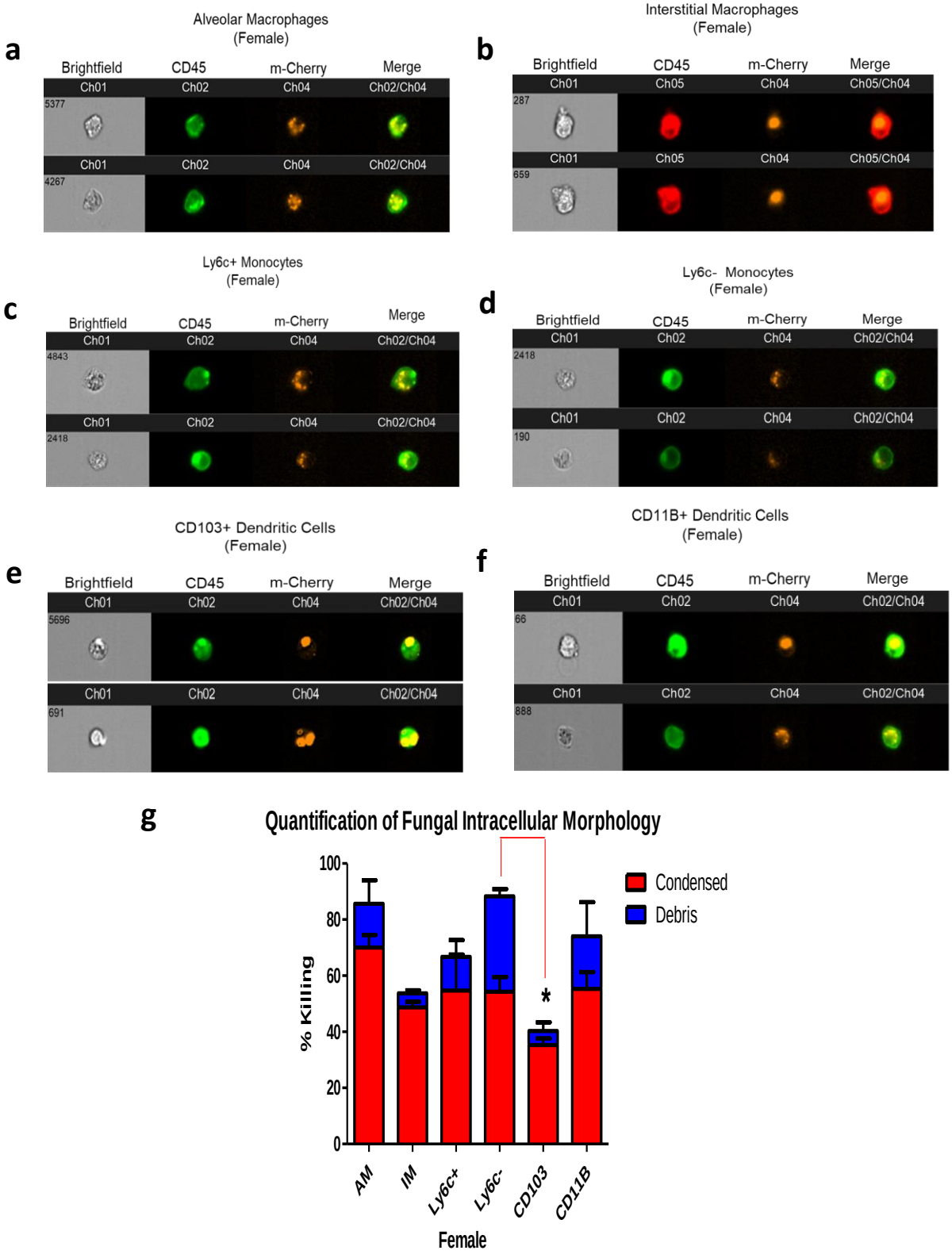
a
Alveolar Macrophages
(Female)
Brightfield
CD45
m-Cherry
Merge
Ch01
Ch02
Ch04
Ch02/Ch04
5377
4267
b
Interstitial Macrophages
(Female)
Ch05
Ch05/Ch04
287
659
c
Ly6c+ Monocytes
(Female)
4843
2418
d
Ly6c- Monocytes
(Female)
190
e
CD103+ Dendritic Cells
(Female)
5696
691
f
CD11B+ Dendritic Cells
(Female)
66
888
g
Quantification of Fungal Intracellular Morphology
% Killing
100
80
60
40
20
0
Condensed
Debris
*
AM
IM
Ly6c+
Ly6c-
CD103
CD11B
Female

Debris $p < .05$	Condensed $p < .05$
IM- Ly6c-: ***	AM – IM: *
Ly6c+ - Ly6c-: *	AM – CD103: **
Ly6c- - CD103: **	IM – CD103: *
	Ly6c- - CD103: *
	CD11B – CD103: ****

Figure 8. Murine pulmonary female phagocyte subsets display varying cryptococcal morphologies after *C. neformans* internalization. Using female BALB/c mice, phagocyte subsets were purified and incubated with m-cherry expressing *C. neoformans* (KN99mCH) for 2hrs at 37°C, 5% CO_2 at a ratio of 20:1. Following incubation, cells were stained for surface markers visualized at 40x magnification by the ImageStreamX-Imaging Flow Cytometer-MKII (Luminex). Figure 8a-8f display cryptococcal morphologies within each pulmonary phagocyte subset. Data of cryptococcal morphology were quantified using IDEAS Software 6.2 and graphically expressed using GraphPad Prism (8g). The data are means ± standard errors of the means (SEM) for three independent experiments. One-way ANOVA with Tukey's post-test was used to detect statistical differences (*,**,***) between groups, $p < 0.05,0.01,0.001$, respectively.

3.4 Murine phagocyte fungicidal activity is not dependent upon phagocyte polarization

In order to determine if exposure to *C. neoformans* induced polarization of macrophage or DC subsets following cryptococcal exposure, cytokine production was examined. Following a 2-hour incubation with *C. neoformans,* cytokines present in the supernatants were assayed using the Bio-Plex Pro Mouse Cytokine 23-plex (BioRad). Detected (Th1/Th2, pro-inflammatory, chemokine) cytokine levels from each subset were quantified as shown in figure 9. Cytokine and chemokine levels were tested for both male and female pulmonary phagocyte subset populations alone and

when incubated with *C. neoformans* strain H99. When analyzing Th1/Th2 associated cytokine levels (Il-12p70, IFN-γ, IL-13), neither male nor female phagocyte subsets displayed any significant differences when comparing the phagocyte population alone and when incubated with *C. neoformans* strain H99 as shown in figure 9a and figure 9b. Next, when analyzing pro-inflammatory cytokines (IL-1a, TNF-α) male phagocyte subsets did not displayed any significant differences in secretion when comparing phagocyte populations alone and when incubated with *C. neoformans* strain H99 (figure 9c). When analyzing female phagocyte subset populations there was a significant decrease in the amount of IL-1a secretion when comparing the alveolar macrophage population alone to alveolar macrophages when incubated with *C. neoformans* strain H99 (figure 9d). Lastly, when analyzing chemokines (MIP-1α, MCP-1) neither male nor female phagocyte subset populations displayed any significant differences in secretion when comparting phagocyte populations alone and when incubated with *C. neoformans* strain H99 as shown in figure 9e and figure 9f. The results indicate that phagocyte polarization is not responsible for the differences in fungicidal activity exhibited by pulmonary macrophage and dendritic cell subpopulations ex vivo.

Th1/Th2

a **Male**

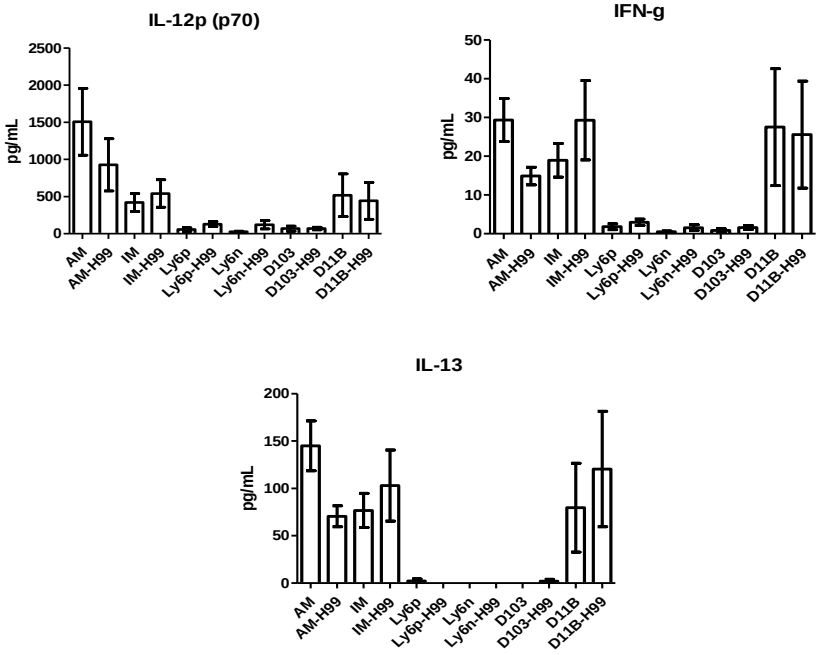

b **Female**

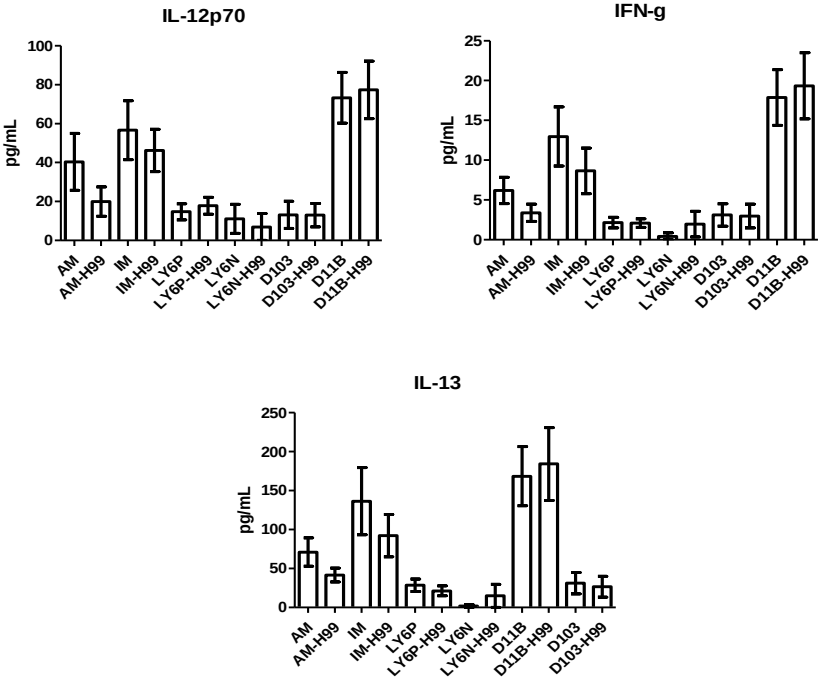

Pro-inflammatory

Male

Female

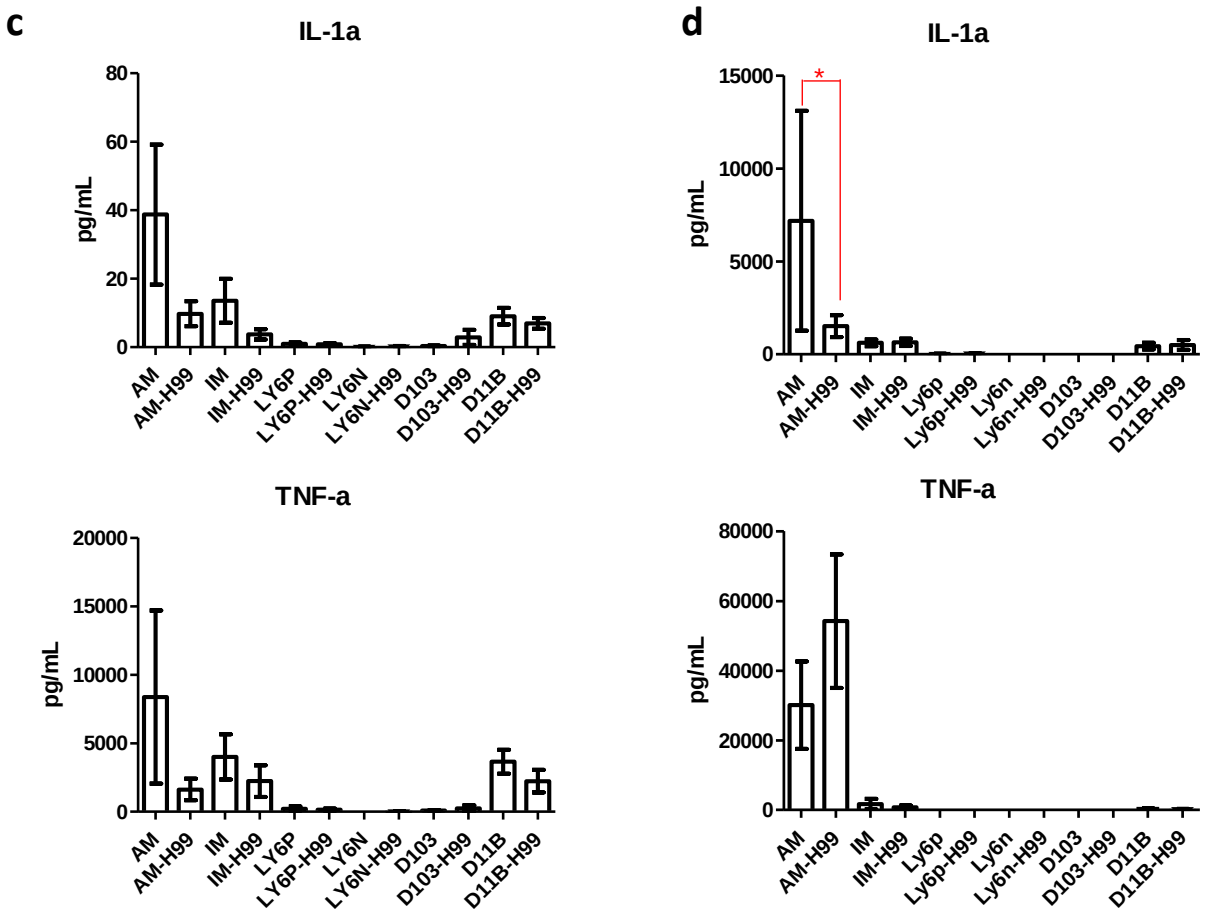

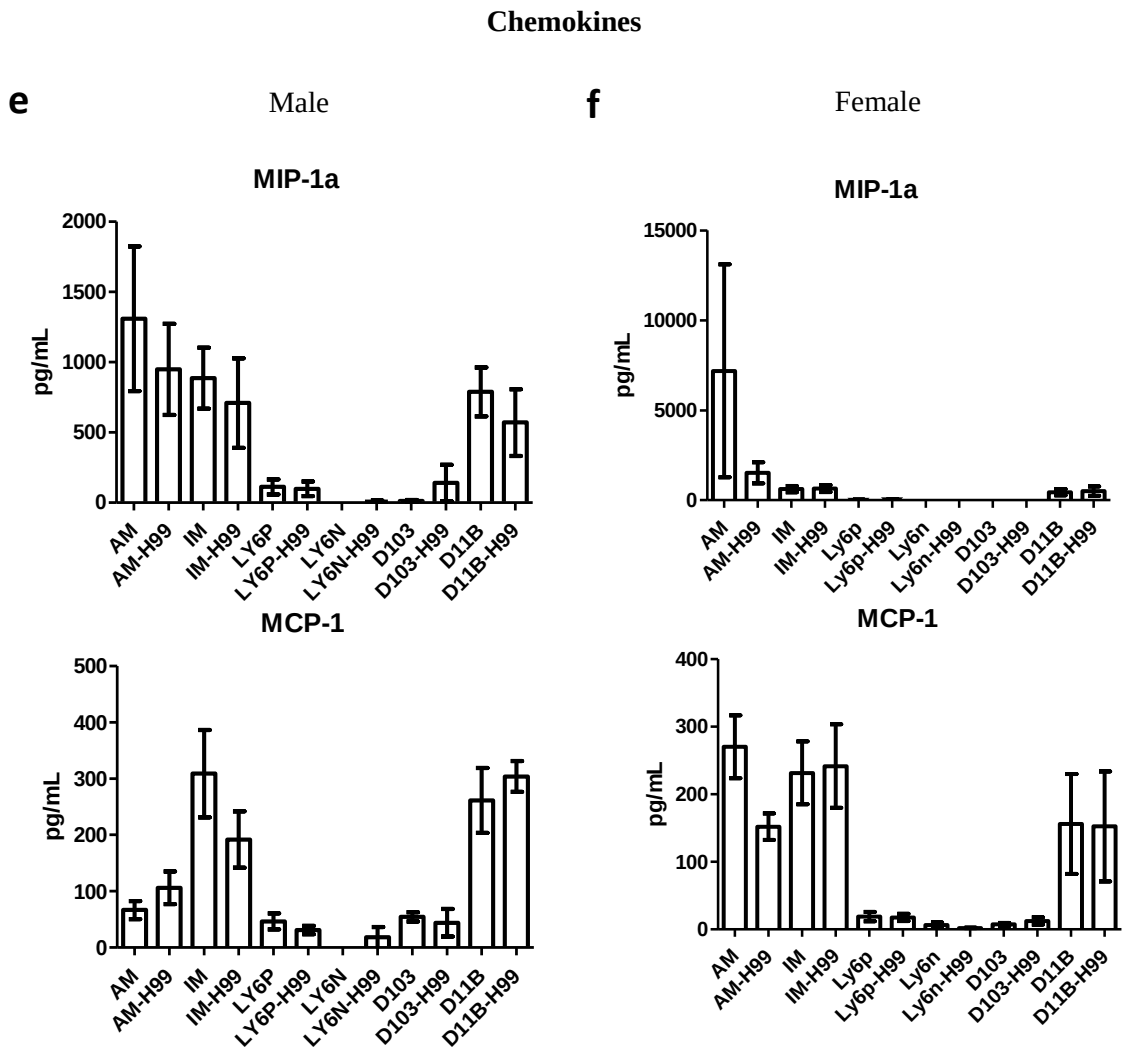

Figure 9. Pulmonary phagocyte cytokine production following incubation with *C. neoformans*. Murine pulmonary macrophages and DCs were harvested and purified using magnetic separation. Cell subsets were incubated at a 20:1 ratio with *C. neoformans* for 2h at 37°C, 5% CO_2 then supernatants were collected. Samples were treated with protease inhibitor and frozen at -80°C until analysis. Samples were analyzed for cytokines/chemokines by Bioplex. Graph (a) and graph (b) shows Th1/Th2 cytokine secretion in pg/ml from both male and female phagocyte subsets alone and when incubated with *C. neoformans* strain H99, respectively. Graph (c) and graph (d) shows pro-inflammatory cytokine secretion in pg/ml from both male and female

phagocyte subsets alone and when incubated with *C. neoformans* strain H99, respectively. Graph (e) and graph (f) shows chemokine secretion from both male and female phagocyte subsets alone and when incubated with *C. neoformans* strain H99, respectively. Data are shown as pg/ml ± standard errors of the means (SEM) from 3 independent experiments from male mice and 3 experiments from female mice. AM = alveolar macrophages, IM = interstitial macrophages, LY6N = $Ly6c^-$ monocyte-like macrophages, LY6P= $Ly6C^+$ positive monocyte-like macrophages, CD11b = $CD11b^+$ dendritic cells, CD103 = $CD103^+$ dendritic cells. ***** indicates $p < 0.05$ (subset alone compared to subset + H99).

3.5 RNA sequencing analysis of murine pulmonary phagocytes displayed differences in transcriptional profiles within permissive and non-permissive phagocytes

After identification of phagocyte subsets with different antifungal activity from male and female BALB/c mice, we were interested in identifying genes involved in these responses. Following a 2-hour incubation with *C. neoformans*, both male and female phagocyte subsets were sequenced and gene expression was compared between each phagocyte subset when interacting with *C. neoformans* to each subset alone. Permissive vs non permissive phagocytes were compared to identify differentially regulated pathways. As shown in figure 10, using the KEGG Pathway database, immune-associated response pathways, cell adhesion molecules and antigen processing and presentation, were identified within permissive and non-permissive phagocytes and compared. Both $CD11b^+$ DCs from male mice (permissive) and $Ly6c^-$ monocyte-like macrophages (non-permissive) from female mice shared common immune associated signaling pathways that included the cell adhesion molecule pathway and the antigen processing and presentation pathway. Within the cell adhesion molecule pathway, gene expression analysis revealed a down-regulation in MHC-1 (red) within the $CD11b^+$ DCs from male mice (figure 10a). When analyzing the same pathway within $Ly6c^-$ monocyte-like macrophages from female mice, there was an up-regulation in MHC-I (blue) and B7H3 (blue), and down-regulation in both MHC-

II (red) and PVRL2 (red) as shown in figure 10c. In the antigen processing and presentation pathway, within $CD11b^{+}$ DCs from male mice, there was a down regulation in both MHC-I (red) and CALR (red) as shown in figure 10b. When analyzing the same pathway within female mice, there was an upregulation in MHC-I (blue) and a down-regulation in both MHC-II (red) and HLA-DM (red) as shown in figure 10d. Notably, within both shared pathways, MHC-I was significantly down-regulated ($p < 0.05$) within the permissive $CD11b^{+}$ DC subsets from male mice and significantly up-regulated ($p < 0.05$) within $Ly6c^{-}$ monocyte-like macrophage subset from female mice. Using Ingenuity Pathway Analysis (IPA) software, top canonical (active) pathways associated with cell metabolism were predicted and their associated genes were identified for both permissive and non-permissive phagocyte subsets as shown in figure 11 and figure 13. Within permissive phagocytes, five top canonical (active) metabolic pathways were identified that included Acetone Degradation I (to Methylglyoxcal) ($p=1.25E^{-03}$), Nicotine Degradation II ($p=8.60E^{-03}$), Bupropion Degradation ($p=1.21E^{-02}$), Uracil Degradation II (reductive) ($p=2.28E^{-02}$), and Thymine Degradation ($p=2.28E^{-02}$) as shown in figure 11. Within these 5 metabolic pathways, their genes associated within permissive phagocytes were identified along with their up-regulation or down-regulation (+/-) (figure 11). Within non-permissive phagocytes, the top 5 canonical (active) metabolic pathways that were identified included, Netrin Signaling ($p=3.3E^{-03}$), Neuroprotective Role of THOP1 in Alzheimer's Disease ($p=4.31E^{-03}$), MIF-mediated Glycocorticoid Regulation ($p=6.50E^{-03}$), Retinoate Biosynthesis I ($p=6.50E^{-03}$), and the Apelin Muscle Signaling Pathway ($p=8.02E^{-03}$) as shown in figure 13. The specific genes within each of these pathways associated with non-permissive phagocytes were also identified along with their up-regulation or down-regulation (+/-) (figure 13). Within the Ingenuity Pathway Analysis platform, a broader analysis was completed in order to identify over lapping canonical pathways based upon shared significantly differentiated genes within permissive and non-permissive phagocyte subsets (figure 12 and figure 14). Within permissive phagocytes, 25 active metabolic pathways were identified (figure 12). Lines connecting pathways represent metabolic

pathways with shared genes. Figure 12 shows a network of associated metabolic pathways, within permissive phagocytes, based upon shared genes. The most active pathways are ranked from p-values smallest to largest indicated by dark red to light red shading. Within this network the most active pathways, shown in dark red, are Acetone Degradation I (to Methylglyoxal), Nicotine Degradation II, and Bupropion Degradation including lines connecting each pathway to related pathways that have shared genes. Similarly, within non-permissive phagocytes, 25 active metabolic pathways were identified as shown in figure 14. Lines connecting pathways represent metabolic pathways with shared genes. Figure 14 shows a network of associated metabolic pathways within non-permissive phagocytes based upon shared genes. The most active pathways are ranked from p-values smallest to largest indicated by dark red to light red shading, respectively. Within this network the most active pathways, shown in dark red, are Netrin Signaling, Neuroprotective Role of THOP1 in Alzheimer's Disease, and MIF-mediated Glucocorticoid Regulation including lines connecting each pathway to related pathways that have shared genes (figure 13). The results indicate the *C. neoformans* causes distinct transcriptional changes within permissive and non-permissive phagocytes.

Male: CD11b^{+} DCs

a

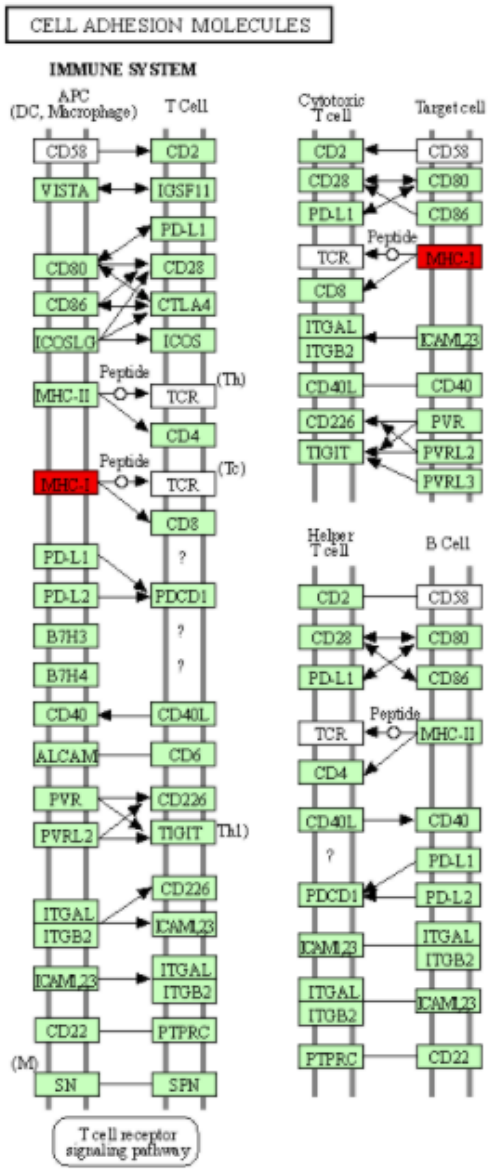

b

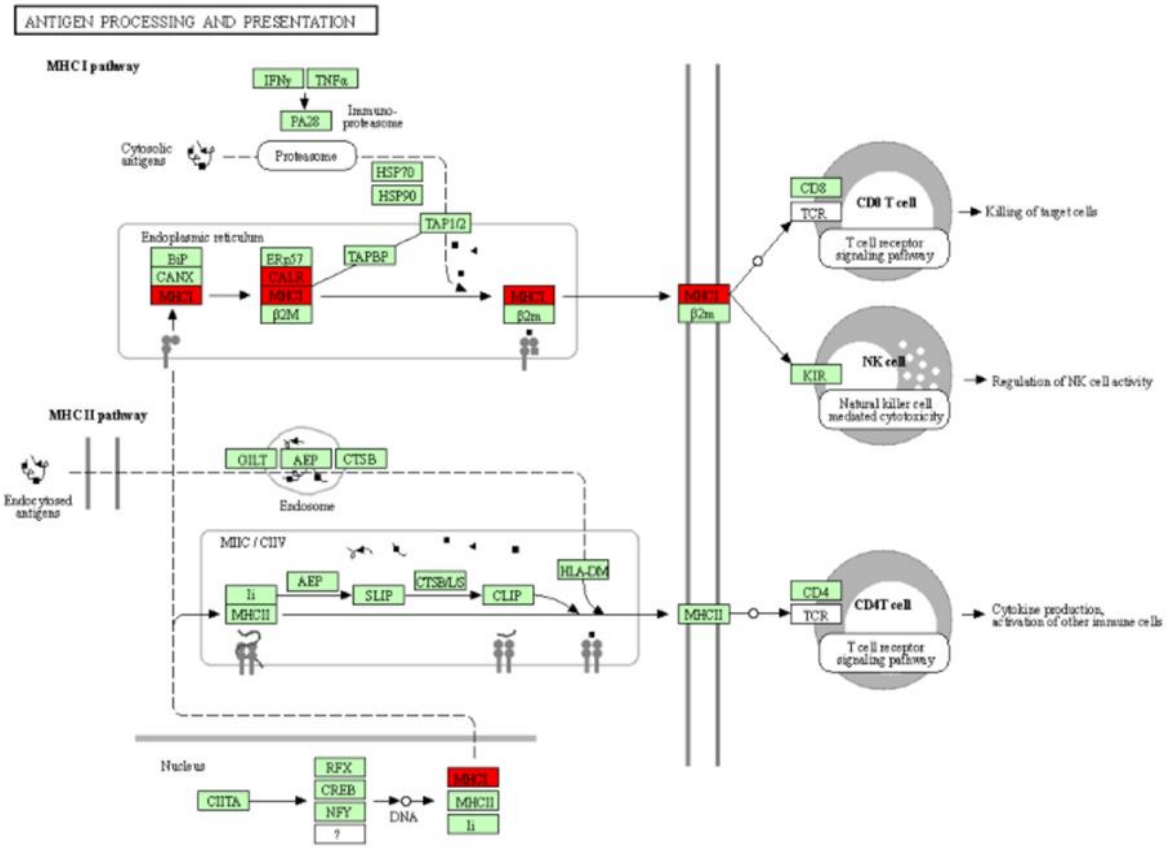
ANTIGEN PROCESSING AND PRESENTATION
MHC I pathway
IFNγ
TNFα
PA28
Immuno-proteasome
Cytosolic antigens
Proteasome
HSP70
HSP90
TAP1/2
Endoplasmic reticulum
BiP
CANX
MHCI
ERp57
CALR
MHCI
β2M
TAPBP
MHCI
β2m
MHCI
β2m
CD8
TCR
CD8 T cell
T cell receptor signaling pathway
Killing of target cells
KIR
NK cell
Natural killer cell mediated cytotoxicity
Regulation of NK cell activity
MHC II pathway
Endocytosed antigens
GILT
AEP
CTSB
Endosome
MIIC / CIIV
Ii
MHCII
AEP
SLIP
CTSB/LS
CLIP
HLA-DM
MHCII
CD4
TCR
CD4T cell
T cell receptor signaling pathway
Cytokine production, activation of other immune cells
Nucleus
CIITA
RFX
CREB
NFY
?
DNA
MHCI
MHCII
Ii

Female: Ly6c^{-} Monocyte-like macrophages

C

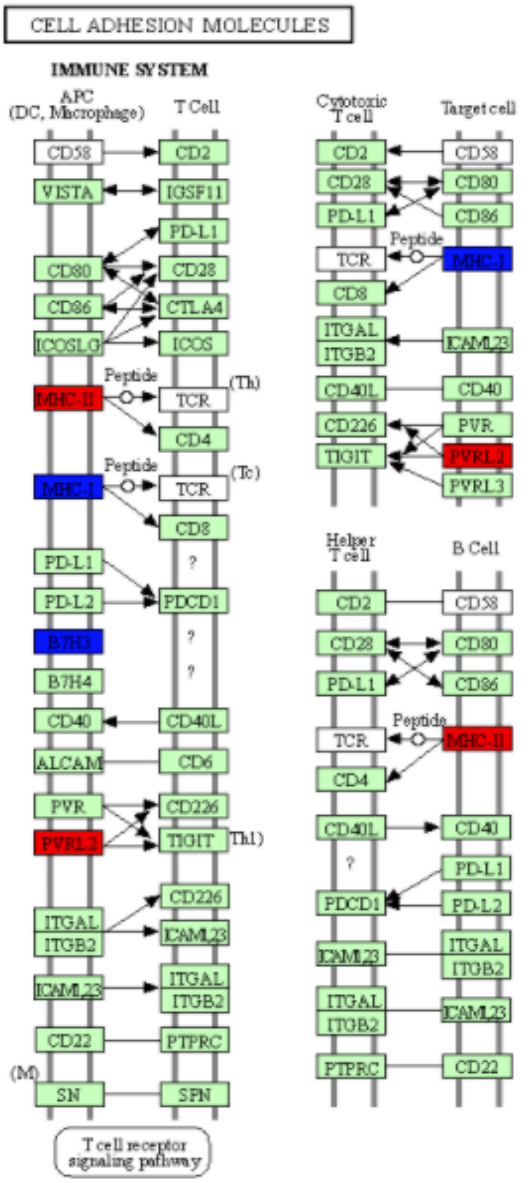

d

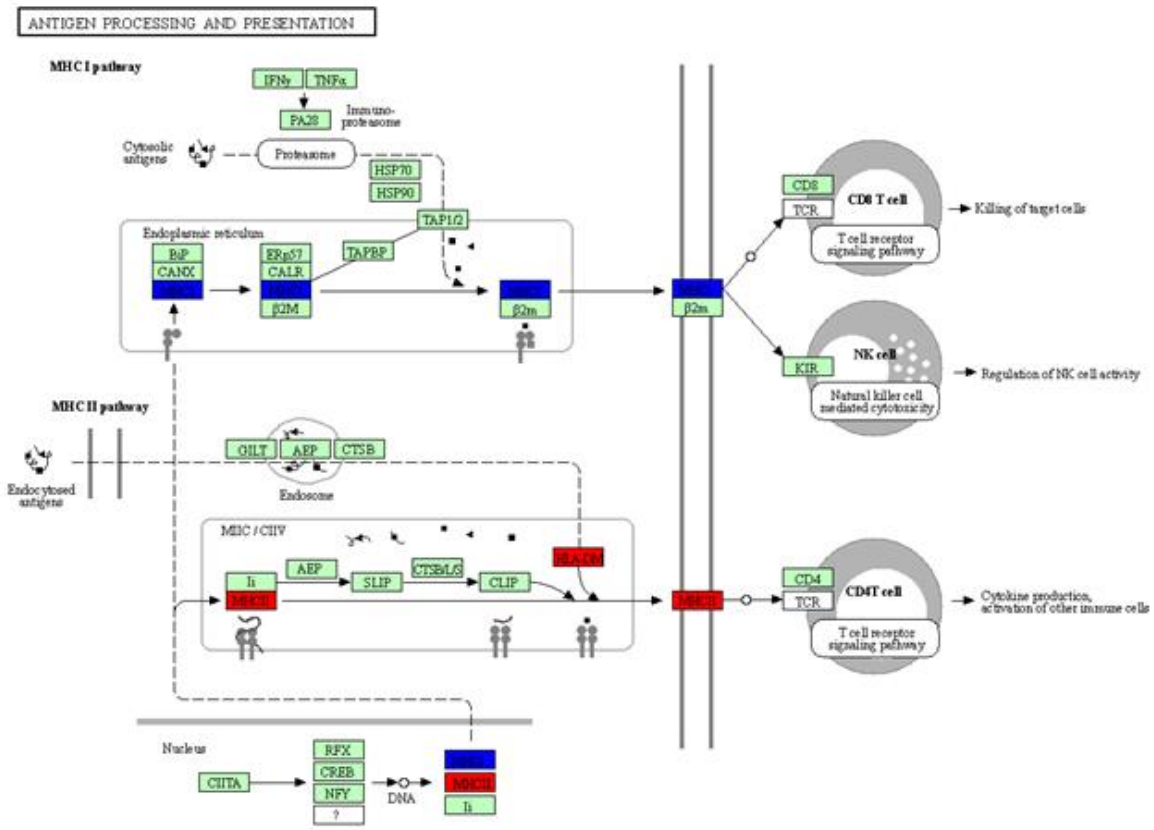

Figure 10. Permissive and non-permissive pulmonary phagocytes exhibit transcriptional differences in immune associated pathways. Using male and female BALB/c mice, phagocyte subsets were purified and incubated with *C. neoformans* strain H99 at 37°C, 5% CO_2 for 2hrs at a ratio of 20:1. Following incubation, cells were collected and stored in TriZol at -20C until analysis. RNA purification and analysis was conducted by Novogene using SMARTer Stranded V2 library prep and samples were sequenced using the Illumina Platform. Differential expression analysis was compared between each macrophage and DC subset alone and when incubated with *C. neoformans* strain H99. Significant differences within gene expression were identified and grouped into signaling pathways using KEGG Pathway Analysis. Figure (a) and figure (b) shows the up-regulation and down-regulation of genes associated with male $CD11b^+$ dendritic cells (DCs) within the cell adhesion molecules and antigen processing and presentation signaling

pathways, respectively. Figure (c) and figure (d) shows the up-regulation and down-regulation of genes associated with female Ly6c- monocyte-like macrophages within the cell adhesion molecules and antigen processing and presentation signaling pathways, respectively. Blue and red represent genes up-regulated or down-regulated, respectively, in $CD11b^{+}$ DCs and $Ly6c^{-}$ monocyte-like macrophages interacting with *C. neoformans* compared to the subset alone. Data were generated from a merged data set from 2 independent female 2 independent male mouse experiments.

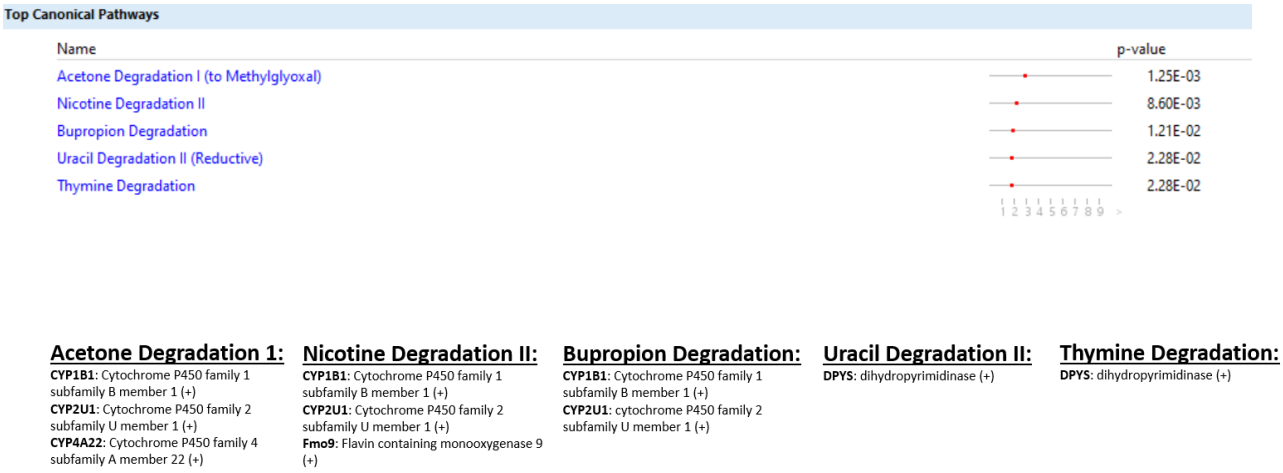

Figure 11. *C. neoformans* leads to the activation of highly specific metabolic pathways within permissive phagocytes. Using male BALB/c mice, phagocyte subsets were purified and incubated with *C. neoformans* strain H99 at 37°C, 5% CO_2 for 2hrs at a ratio of 20:1. Following incubation, cells were collected and stored in TriZol at -20C until analysis. RNA purification and analysis was conducted by Novogene using SMARTer Stranded V2 library prep and samples were sequenced using the Illumina Platform. Differential expression analysis was compared between each macrophage and DC subset alone and when incubated with *C. neoformans* strain H99. Significant differences within gene expression were identified and grouped into predicted canonical pathways using Ingenuity Pathway Analysis (IPA) software. The data show the top five active canonical pathways when comparing male $CD11b^{+}$ DCs interacting with *C. neoformans* to

$CD11b^+$ DCs alone in addition to the specific genes involved within each pathway as shown below. Data were generated from 1 independent male mice experiment.

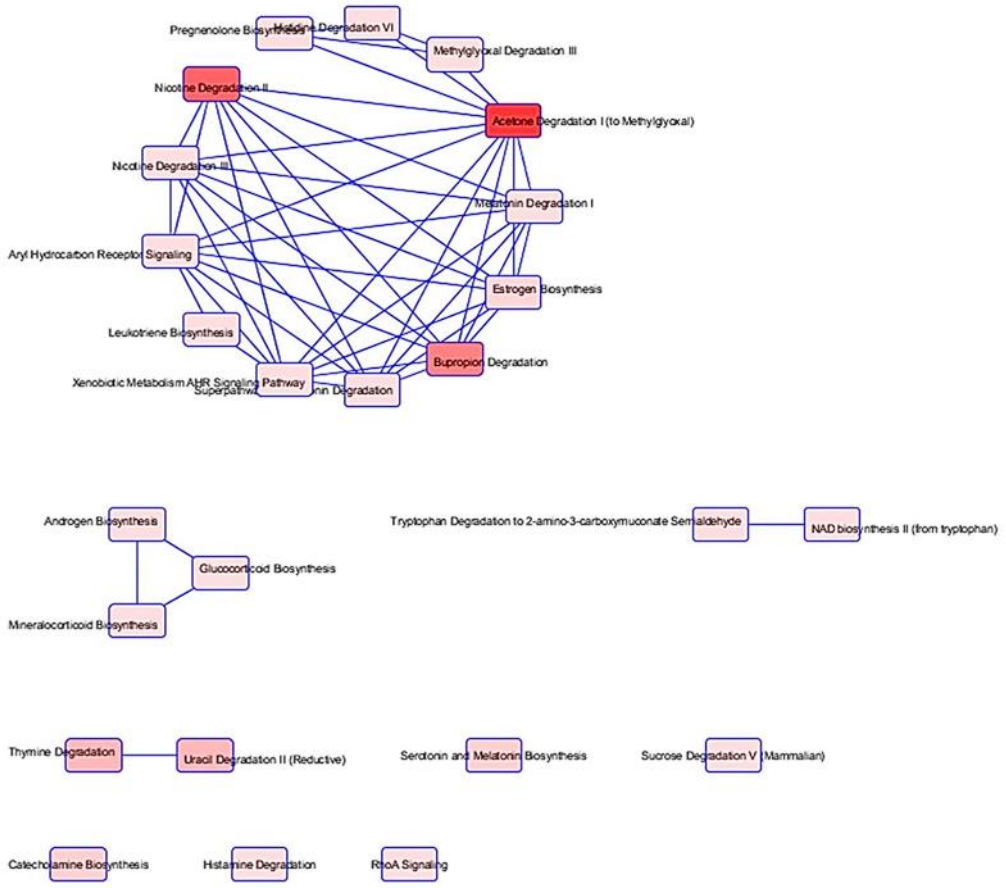

Figure 12. *C. neoformans* leads to a highly differentiated network of associated metabolic pathways within permissive phagocytes. Using male BALB/c mice, phagocyte subsets were purified and incubated with *C. neoformans* strain H99 at 37°C, 5% CO_2 for 2hrs at a ratio of 20:1. Following incubation, cells were collected and stored in TriZol at -20C until analysis. RNA purification and analysis was conducted by Novogene using SMARTer Stranded V2 library prep and samples were sequenced using the Illumina Platform. Differential expression analysis was compared between each macrophage and DC subset alone and when incubated with *C. neoformans* strain H99. Significant differences within gene expression were identified and

grouped into predicted canonical (active) pathways using Ingenuity Pathway Analysis (IPA) software. Associated pathways containing overlapping genes are shown when comparing male CD11b^{+} DCs interacting with *C. neoformans* to CD11b^{+} DCs alone. Boxes shaded from dark red to light red indicate a difference $p < 0.05$ from greatest to least, respectively. Connecting lines indicate pathways with shared genes. Data were generated from 1 independent male mice experiment.

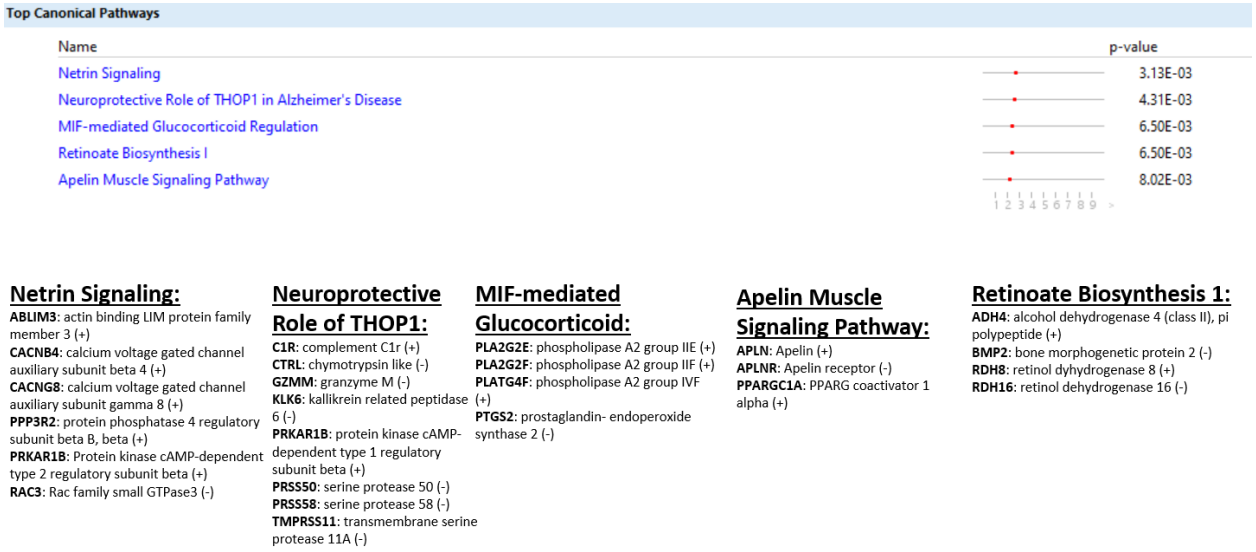

Figure 13. *C. neoformans* leads to the activation of highly specific metabolic pathways within non-permssive phagocytes. Using female BALB/c mice, phagocyte subsets were purified and incubated with *C. neoformans* strain H99 at 37C, 5% CO2 for 2hrs at a ratio of 20:1. Following incubation, cells were collected and stored in TriZol at -20C until analysis. RNA purification and analysis was conducted by Novogene using SMARTer Stranded V2 library prep and samples were sequenced using the Illumina Platform. Differential expression analysis was compared between each macrophage and DC subset alone and when incubated with *C. neoformans* strain H99. Significant differences within gene expression were identified and

grouped into predicted canonical pathways using Ingenuity Pathway Analysis (IPA) software. Fig 10a shows the top five active canonical pathways when comparing female Ly6c$^-$ monocytes interacting with *C. neoformans* to Ly6c$^-$ monocytes alone. Fig 10b shows specific genes that associated within each pathway. Data were generated from 2 independent female mice experiments.

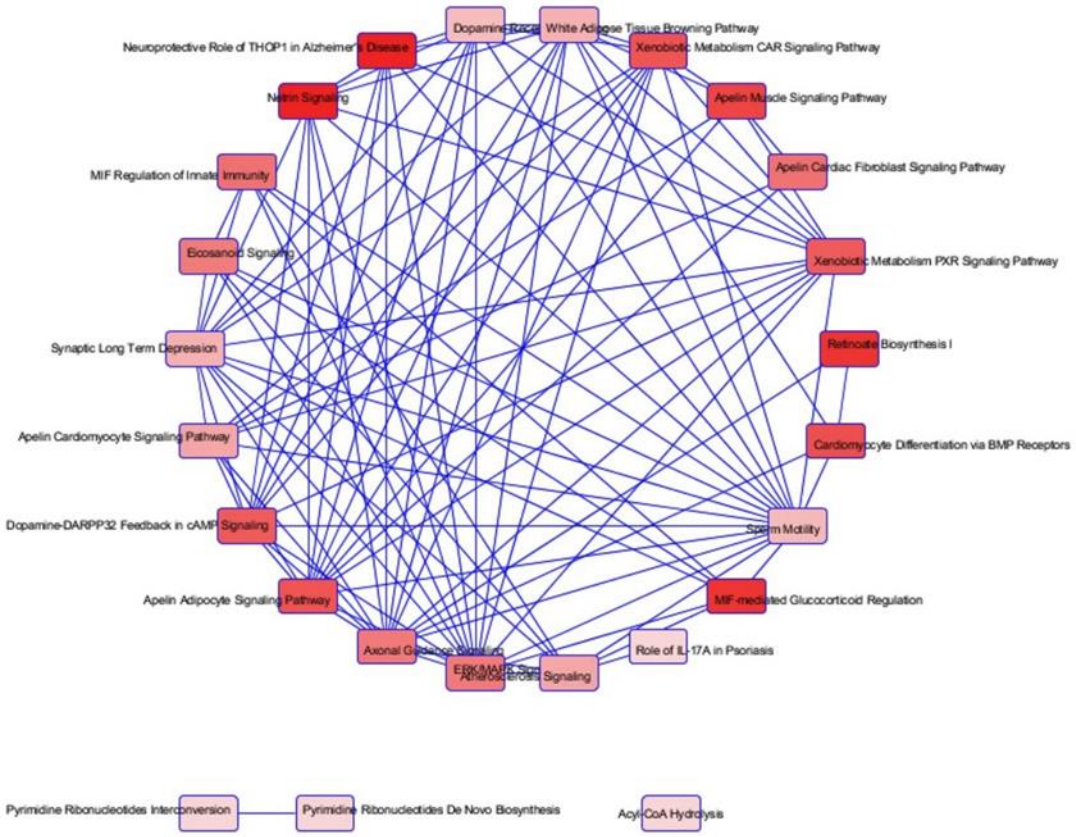

Figure 14. *C. neoformans* leads to a differentiated network of associated metabolic pathways within non-permissive phagocytes. Using male BALB/c mice, phagocyte subsets were purified and incubated with *C. neoformans* strain H99 at 37C, 5% CO_2 for 2hrs at a ratio of 20:1. Following incubation, cells were collected and stored in TriZol at -20C until analysis. RNA purification and analysis was conducted by Novogene using SMARTer Stranded V2 library prep

and samples were sequenced using the Illumina Platform. Differential expression analysis was compared between each macrophage and DC subset alone and when incubated with *C. neoformans* strain H99. Significant differences within gene expression were identified and grouped into predicted canonical (active) pathways using Ingenuity Pathway Analysis (IPA) software. Associated pathways containing overlapping genes are shown when comparing female Ly6c$^-$ monocyte-like macrophages interacting with *C. neoformans* to Ly6c$^-$ monocyte-like macrophages alone. Connecting lines indicate pathways with shared genes. Boxes shaded from dark red to light red indicates a difference $p < 0.05$ from greatest to least, respectively. Data were generated from 2 independent female mice experiments.

CHAPTER IV

DISCUSSION AND CONCLUSION

Although the induction of ART therapy has resulted in declining HIV/AIDS related mortality, *C. neoformans* still remains the leading cause of fungal related death in these patients (Rajasingham et al., 2017). Due to the intracellular nature of *C. neoformans*, the identification of specific mechanisms that mediate intracellular *C. neoformans* survival and replication can aid in the development of novel therapies for the treatment of cryptococcosis. Previous studies have provided an investigation into the intracellular nature of *C. neoformans* and phagocytic cells using peripheral blood mononuclear cells (PBMCs), or macrophage cell lines (De Leon-Rodriguez, Rossi, Fu, Dragotakes, Coelho, Guerrero Ros, et al., 2018; Subramani et al., 2020). In addition, more recent fate-mapping studies have identified macrophage and DC subsets and have defined origins of both human and murine phagocytes (Gordon, Plüddemann, & Martinez Estrada, 2014; Hoffmann et al., 2018; Misharin, 2013) but few have analyzed how these phagocyte subsets initially interact with *C. neoformans (*reviewed in (Nelson et al., 2020)). The bacterial pathogen, *Mycobacterium tuberculosis* (Mtb) has similar lung pathology, can survive intracellularly in macrophages, and his similar protective immune responses to *C. neoformans* (as reviewed in

(Pirofski & Casadevall, 2020; Serbina, Jia, Hohl, & Pamer, 2008)). Studies have shown that alveolar macrophages are more permissive to intracellular bacterial growth as opposed to interstitial macrophages resulting in differences in transcriptional responses upon the interaction with Mtb (Huang, Nazarova, & Russell, 2019; Huang, Nazarova, Tan, Liu, & Russell, 2018; Pisu, Huang, Grenier, & Russell, 2020).

In our study, we first examined the fungicidal activity of each murine pulmonary phagocyte subsets. We demonstrated that pulmonary phagocyte subsets respond differently upon interaction with *C. neoformans*. Additionally, it has been observed that males are more affected by *C. neformans* related infection more frequently and more severely than females (as reviewed in (Guess, Rosen, & McClelland, 2018). Furthermore, the requirement to study sex as a biological variable led us to conduct these experiments in both male and female mice. We then noticed differences in data generated from male mice compared to female mice, which led to the further examination of our data through stratification by sex. Once our data was stratified by sex, results showed a significant decrease in the amount of cryptococcal growth when *C. neoformans* strain H99 was incubated with female Ly6c- monocyte-like macrophages as compared to the H99 control. However, this was not seen within the male phagocyte population. In a reversible hepatic fibrosis murine model, it was shown that Ly6c$^-$ monocyte like-macrophages played a crucial role in resolving inflammation and showed an enrichment for pathways related to lysosomes, endocytosis and antigen presentation which are implicated in phagocytosis (Butenko et al., 2020; Ramachandran et al., 2012). Female Ly6c$^-$ monocyte-like macrophages could exhibit a similar role in resolving pulmonary

inflammation and controlling cryptococcal growth during a *C. neoformans* infection. Based on these results several studies were initiated to confirm these findings and to gain more insight into the *C. neoformans* and pulmonary phagocyte interaction.

In our studies, an association analysis was performed with the use of flow cytometry in order to verify that each pulmonary phagocyte subset was able to interact with *C. neoformans*, and that our antifungal activity was not biased by the lack of interaction by individual subsets. We confirmed that all murine pulmonary phagocyte subsets interacted with *C. neoformans* ex vivo to a similar degree. Therefore, our differences in antifungal activity were not attributable to differences in degree of phagocyte-cryptococcal interactions. To our knowledge, we are the first to examine each specific pulmonary phagocyte subset to determine their individual interactions with *C. neoformans*, and we are also the first to observe sex differences in pulmonary phagocyte antifungal activity.

To observe early pulmonary phagocyte-cryptococcal interaction, we conducted an imaging flow cytometric analysis. This technology allowed us to quantify intracellular morphologies within each subset. We did not observe significant differences in fungicidal activity in phagocytes from male mice. However, these data are from a 2 hr interaction, and as evidenced by our 24hr antifungal assays, these phenotypes change over the course of the incubation period.

Previous literature has shown that phagocyte polarization phagocyte polarization (specifically macrophage polarization) is critical for controlling cryptococcal infection. Protective responses in a murine vaccination model are highly dependent upon cell mediated Th1-type immune responses resulting in M1 macrophage polarization (Hardison et al., 2010; He et al., 2012; Y. Zhang et al.,

2009). Permissive growth of *C. neoformans* is related to the induction of a Th2-type response, leading to the induction of M2 macrophage polarization and disease exacerbation (Müller et al., 2008; Osterholzer, Surana, et al., 2009). In our study we performed a cytokine analysis using each pulmonary phagocyte subset in order to identify possible phagocyte polarization. In cells from both male and female mice, we did not observe any significant decreases in the amount of secreted Th1/Th2 associated cytokines IL-12p40, IL-13, and IFN-γ or chemokines MIP-1a and MCP-1 when comparing phagocyte subsets alone and when incubated with *C. neoformans* strain H99. Similarly, when observing pro-inflammatory cytokine secretion of IL-1a and TNF-a there were no differences seen in cytokine secretion within the male phagocyte population alone and when incubated with *C. neoformans* strain H99. However, within female mice there was a significant decrease in secretion of pro-inflammatory IL-1a when alveolar macrophages were incubated with *C. neoformans* strain H99. Though neither of the other female phagocyte subsets displayed any observed differences in IL-1a and TNF-a secretion. Although we did observe some changes in overall cytokine production by pulmonary phagocytes, none correlated to polarization of macrophages or DCs. Therefore, we concluded that phagocyte polarization is not responsible for the differences in antifungal activity observed by some subsets.

In order to analyze differences within the transcriptional profiles of permissive and non-permissive phagocyte subsets, we conducted an RNA sequencing analysis comparing each phagocyte subset upon the interaction with *C. neoformans* to the subset alone. Within permissive and non-permissive phagocytes, we discovered a large network of differentiated metabolic pathways sharing common

genes that were significantly up-regulated and down-regulated. Further studies are needed to provide a more in-depth analysis into these pathways in order to determine their involvement in regard to fungicidal activity within permissive and non-permissive phagocytes. In addition, within the permissive male phagocyte subset $CD11b^+$ DCs we observed a significant down regulation with MHC-1 associated with immune response, antigen processing and presentation and cell adhesion molecules. Interestingly, this expression greatly contrasted within the non-permissive female Ly6c- monocyte-like macrophages which exhibited an upregulation in MHC-1. The major histocompatibility (MHC) class 1 antigen presentation pathway plays a vital role in adaptive immunity by recognizing and alerting the immune system to virally infected cells as reviewed in (Hewitt, 2003). MHC Class I molecules are present on the cell surface of all nucleated cells as reviewed in (Muntjewerff, Meesters, Bogaart, & Revelo, 2020) and function to present foreign and antigenic peptides primarily to $CD8^+$ T lymphocytes for defense against intracellular pathogens (Cruz, Colbert, Merino, Kriegsman, & Rock, 2017; Embgenbroich & Burgdorf, 2018; Wieczorek et al., 2017). Evidence that permissive phagocytes show a down-regulation in MHC class I serves as indicator that *C. neoformans* leads to transcriptional changes which may contribute in a deficiency in vital immune cell machinery that aids to control and eliminate the fungal pathogen. Our pathway analysis, revealed top pathways activated, related to various metabolic functioning, within permissive and non-permissive phagocytes. An overlapping pathway analysis was conducted in order to identify related pathways based upon differentially expressed gene overlapping. The results revealed multiple distinct metabolic pathways linked by common gene similarities. We concluded that *C. neoformans* leads to differential gene expression affecting

multiple metabolic pathways. This information can serve as roadmap to target genes that are resulting in the difference in fungicidal capabilities within pulmonary murine phagocytes.

To our knowledge, our studies have provided the first examination of individual phagocyte subset interactions with *C. neoformans*. The results from these studies lead us to conclude that different populations of murine pulmonary phagocytes interact differently with *C. neoformans*, and these differences depend upon sex of the murine host and differential gene expression, but are not dependent on phagocyte polarization. Future studies using gene knockout mice for pulmonary *C. neoformans* infection will be needed to provide further insight into the functional aspects of genes and signaling pathways identified in these studies. This will guide our studies to eventually target specific genes/pathways for use to prevent intracellular replication and trafficking of *C. neoformans* to the brain in order to prevent meningitis. The results from this study indicate the need for additional research into pulmonary phagocyte subsets and their interactions with intracellular pathogens.

References

Alanio, A., Desnos-Ollivier, M., & Dromer, F. (2011). Dynamics of Cryptococcus neoformans-macrophage interactions reveal that fungal background influences outcome during cryptococcal meningoencephalitis in humans. *mBio, 2*(4). doi:10.1128/mBio.00158-11

Alvarez, M., & Casadevall, A. (2007). Cell-to-cell spread and massive vacuole formation after Cryptococcus neoformans infection of murine macrophages. *BMC immunology, 8*, 16-16. doi:10.1186/1471-2172-8-16

Arora, S., Hernandez, Y., Erb-Downward, J. R., McDonald, R. A., Toews, G. B., & Huffnagle, G. B. (2005). Role of IFN-gamma in regulating T2 immunity and the development of alternatively activated macrophages during allergic bronchopulmonary mycosis. *Journal of immunology (Baltimore, Md. : 1950), 174*(10), 6346-6356. doi:10.4049/jimmunol.174.10.6346

Arora, S., Olszewski, MA, Tsang, TM, McDonald, RA, Toews, GB, Huffnagle, GB. (2011). Effect of Cytokine Interplay on Macrophage Polarization during Chronic Pulmonary Infection with Cryptococcus neoformans. *Infection and Immunity, 79*, 1915–1926. doi:10.1128/IAI.01270-10

Arras, S. D. M., Chitty, J. L., Wizrah, M. S. I., Erpf, P. E., Schulz, B. L., Tanurdzic, M., & Fraser, J. A. (2017). Sirtuins in the phylum Basidiomycota: A role in virulence in Cryptococcus neoformans. *Scientific Reports, 7*, 46567-46567. doi:10.1038/srep46567

Baddley, J. W., Perfect, J. R., Oster, R. A., Larsen, R. A., Pankey, G. A., Henderson, H., . . . Pappas, P. G. (2008). Pulmonary cryptococcosis in patients without HIV infection: factors associated with disseminated disease. *Eur J Clin Microbiol Infect Dis, 27*(10), 937-943. doi:10.1007/s10096-008-0529-z

Beaty, S. R., Rose, C. E., & Sung, S.-s. J. (2007). Diverse and Potent Chemokine Production by Lung CD11b^{high} Dendritic Cells in Homeostasis and in Allergic Lung Inflammation. *The Journal of Immunology, 178*(3), 1882-1895. doi:10.4049/jimmunol.178.3.1882

Bicanic, T., Bottomley, C., Loyse, A., Brouwer, A. E., Muzoora, C., Taseera, K., . . . Jarvis, J. N. (2015). Toxicity of Amphotericin B Deoxycholate-Based Induction Therapy in Patients with HIV-Associated Cryptococcal Meningitis. *Antimicrobial agents and chemotherapy, 59*(12), 7224-7231. doi:10.1128/AAC.01698-15

Bojarczuk, A., Miller, K. A., Hotham, R., Lewis, A., Ogryzko, N. V., Kamuyango, A. A., . . . Johnston, S. A. (2016). Cryptococcus neoformans Intracellular Proliferation and Capsule Size Determines Early Macrophage Control of Infection. *Scientific reports, 6*, 21489-21489. doi:10.1038/srep21489

Butenko, S., Satyanarayanan, S. K., Assi, S., Schif-Zuck, S., Sher, N., & Ariel, A. (2020). Transcriptomic Analysis of Monocyte-Derived Non-Phagocytic Macrophages Favors a Role in Limiting Tissue Repair and Fibrosis. *Frontiers in immunology, 11*, 405. doi:10.3389/fimmu.2020.00405

Carrillo-Muñoz, A. J., Giusiano, G., Ezkurra, P. A., & Quindós, G. (2006). Antifungal agents: mode of action in yeast cells. *Rev Esp Quimioter, 19*(2), 130-139.

Chaka, W., Verheul, A. F., Vaishnav, V. V., Cherniak, R., Scharringa, J., Verhoef, J., . . . Hoepelman, I. M. (1997). Cryptococcus neoformans and cryptococcal glucuronoxylomannan, galactoxylomannan, and mannoprotein induce different levels of tumor necrosis factor alpha in human peripheral blood mononuclear cells. *Infection and immunity, 65*(1), 272-278. doi:10.1128/iai.65.1.272-278.1997

Chang, Y. C., & Kwon-Chung, K. J. (1994). Complementation of a capsule-deficient mutation of Cryptococcus neoformans restores its virulence. *Mol Cell Biol, 14*(7), 4912-4919. doi:10.1128/mcb.14.7.4912

Chayakulkeeree, M., & Perfect, J. R. (2006). Cryptococcosis. *Infect Dis Clin North Am, 20*(3), 507-544, v-vi. doi:10.1016/j.idc.2006.07.001

Chen, G. H., Teitz-Tennenbaum, S., Neal, L. M., Murdock, B. J., Malachowski, A. N., Dils, A. J., . . . Osterholzer, J. J. (2016). Local GM-CSF-dependent differentiation and activation of pulmonary dendritic cells and macrophages protect against progressive cryptococcal lung infection in mice. *Journal of Immunology, 196*(4), 1810-1821. doi:10.4049/jimmunol.1501512

Cherniak, R., Jones, R. G., & Reiss, E. (1988). Structure determination of Cryptococcus neoformans serotype A-variant glucuronoxylomannan by 13C-n.m.r. spectroscopy. *Carbohydr Res, 172*(1), 113-138. doi:10.1016/s0008-6215(00)90846-2

Cheung, D. O. Y., Halsey, K., & Speert, D. P. (2000). Role of Pulmonary Alveolar Macrophages in Defense of the Lung against <em>Pseudomonas aeruginosa</em&gt. *Infection and immunity, 68*(8), 4585. doi:10.1128/IAI.68.8.4585-4592.2000

Condon, T. V., Sawyer, R. T., Fenton, M. J., & Riches, D. W. (2011). Lung dendritic cells at the innate-adaptive immune interface. *J Leukoc Biol, 90*(5), 883-895. doi:10.1189/jlb.0311134

Cox, G. M., Harrison, T. S., McDade, H. C., Taborda, C. P., Heinrich, G., Casadevall, A., & Perfect, J. R. (2003). Superoxide dismutase influences the virulence of Cryptococcus

neoformans by affecting growth within macrophages. *Infection and immunity, 71*(1), 173-180. doi:10.1128/iai.71.1.173-180.2003

Cruz, F. M., Colbert, J. D., Merino, E., Kriegsman, B. A., & Rock, K. L. (2017). The Biology and Underlying Mechanisms of Cross-Presentation of Exogenous Antigens on MHC-I Molecules. *Annual review of immunology, 35*, 149-176. doi:10.1146/annurev-immunol-041015-055254

D'Souza, C. A., Kronstad, J. W., Taylor, G., Warren, R., Yuen, M., Hu, G., . . . Cuomo, C. A. (2011). Genome variation in Cryptococcus gattii, an emerging pathogen of immunocompetent hosts. *mBio, 2*(1), e00342. doi:10.1128/mBio.00342-10

Davis, M. J., Eastman, A. J., Qiu, Y., Gregorka, B., Kozel, T. R., Osterholzer, J. J., . . . Olszewski, M. A. (2015). Cryptococcus neoformans-induced macrophage lysosome damage crucially contributes to fungal virulence. *Journal of Immunology, 194*(5), 2219-2231. doi:10.4049/jimmunol.1402376

Davis, M. J., Tsang, T. M., Qiu, Y., Dayrit, J. K., Freij, J. B., Huffnagle, G. B., & Olszewski, M. A. (2013). Macrophage M1/M2 polarization dynamically adapts to changes in cytokine microenvironments in Cryptococcus neoformans infection. *mBio, 4*(3). doi:10.1128/mBio.00264-13

Day, J. N., Chau, T. T. H., Wolbers, M., Mai, P. P., Dung, N. T., Mai, N. H., . . . Farrar, J. J. (2013). Combination antifungal therapy for cryptococcal meningitis. *N Engl J Med, 368*(14), 1291-1302. doi:10.1056/NEJMoa1110404

De Leon-Rodriguez, C. M., Rossi, D. C. P., Fu, M. S., Dragotakes, Q., Coelho, C., Guerrero Ros, I., . . . Casadevall, A. (2018). The Outcome of the Cryptococcus neoformans-Macrophage Interaction Depends on Phagolysosomal Membrane Integrity. *J Immunol, 201*(2), 583-603. doi:10.4049/jimmunol.1700958

De Leon-Rodriguez, C. M., Rossi, D. C. P., Fu, M. S., Dragotakes, Q., Coelho, C., Ros, I. G., . . . Casadevall, A. (2018). The outcome of the cryptococcus neoformans–macrophage interaction depends on phagolysosomal membrane integrity. *Journal of Immunology, 201*(2), 583-603. doi:10.4049/jimmunol.1700958

Decote-Ricardo, D., LaRocque-de-Freitas, I. F., Rocha, J. D. B., Nascimento, D. O., Nunes, M. P., Morrot, A., . . . Freire-de-Lima, C. G. (2019). Immunomodulatory Role of Capsular Polysaccharides Constituents of Cryptococcus neoformans. *Frontiers in medicine, 6*, 129-129. doi:10.3389/fmed.2019.00129

Ellis, D., & Pfeiffer, T. (1992). The ecology of Cryptococcus neoformans. *Eur J Epidemiol, 8*(3), 321-325. doi:10.1007/bf00158562

Ellis, D. H. (1987). Cryptococcus neoformans var. gattii in Australia. *J Clin Microbiol, 25*(2), 430-431. Retrieved from https://jcm.asm.org/content/jcm/25/2/430.full.pdf

Ellis, D. H., & Pfeiffer, T. J. (1990). Natural habitat of Cryptococcus neoformans var. gattii. *J Clin Microbiol, 28*(7), 1642-1644. Retrieved from https://jcm.asm.org/content/jcm/28/7/1642.full.pdf

Embgenbroich, M., & Burgdorf, S. (2018). Current Concepts of Antigen Cross-Presentation. *Frontiers in immunology, 9*, 1643-1643. doi:10.3389/fimmu.2018.01643

Epelman, S., Lavine, K. J., & Randolph, G. J. (2014). Origin and functions of tissue macrophages. *Immunity, 41*(1), 21-35. doi:10.1016/j.immuni.2014.06.013

Espinosa, V., & Rivera, A. (2016). First Line of Defense: Innate Cell-Mediated Control of Pulmonary Aspergillosis. *Front Microbiol, 7*, 272. doi:10.3389/fmicb.2016.00272

Feldmesser, M., Kress, Y., Novikoff, P., & Casadevall, A. (2000). Cryptococcus neoformans is a facultative intracellular pathogen in murine pulmonary infection. *Infection and Immunity, 68*(7), 4225-4237. doi:10.1128/IAI.68.7.4225-4237.2000

Feretzaki, M., Hardison, S. E., Wormley, F. L., Jr., & Heitman, J. (2014). Cryptococcus neoformans hyperfilamentous strain is hypervirulent in a murine model of cryptococcal meningoencephalitis. *PLoS One, 9*(8), e104432. doi:10.1371/journal.pone.0104432

Fisher, K. M., Montrief, T., Ramzy, M., Koyfman, A., & Long, B. (2021). Cryptococcal meningitis: a review for emergency clinicians. *Internal and Emergency Medicine*. doi:10.1007/s11739-020-02619-2

Franzot, S. P., Fries, B. C., Cleare, W., & Casadevall, A. (1998). Genetic Relationship between Cryptococcus neoformans var. neoformans Strains of Serotypes A and D. *Journal of Clinical Microbiology, 36*(8), 2200. Retrieved from http://jcm.asm.org/content/36/8/2200.abstract

Furuhashi, K., Suda, T., Hasegawa, H., Suzuki, Y., Hashimoto, D., Enomoto, N., . . . Chida, K. (2012). Mouse Lung CD103+ and CD11bhigh Dendritic Cells Preferentially Induce Distinct CD4+ T-Cell Responses. *American Journal of Respiratory Cell and Molecular Biology, 46*(2), 165-172. doi:10.1165/rcmb.2011-0070OC

Gautier, E. L., Chow, A., Spanbroek, R., Marcelin, G., Greter, M., Jakubzick, C., . . . Randolph, G. J. (2012). Systemic analysis of PPARgamma in mouse macrophage populations reveals marked diversity in expression with critical roles in resolution of inflammation and airway immunity. *J Immunol, 189*(5), 2614-2624. doi:10.4049/jimmunol.1200495

Ghaffar, M., Orr, C., & Webb, G. (2019). Antiphagocytic protein 1 increases the susceptibility of Cryptococcus neoformans to amphotericin B and fluconazole. *PLOS ONE, 14*(12), e0225701. doi:10.1371/journal.pone.0225701

Gibbings, S. L., & Jakubzick, C. V. (2018). Isolation and Characterization of Mononuclear Phagocytes in the Mouse Lung and Lymph Nodes. *Methods Mol Biol, 1809*, 33-44. doi:10.1007/978-1-4939-8570-8_3

Gibbings, S. L., Thomas, S. M., Atif, S. M., McCubbrey, A. L., Desch, A. N., Danhorn, T., . . . Jakubzick, C. V. (2017). Three unique interstitial macrophages in the murine lung at steady state. *American Journal of Respiratory Cell and Molecular Biology, 57*(1), 66-76. doi:10.1165/rcmb.2016-0361OC

Gordon, S., Plüddemann, A., & Martinez Estrada, F. (2014). Macrophage heterogeneity in tissues: phenotypic diversity and functions. *Immunological reviews, 262*(1), 36-55. doi:10.1111/imr.12223

Grahnert, A., Richter, T., Piehler, D., Eschke, M., Schulze, B., Muller, U., . . . Alber, G. (2014). IL-4 receptor-alpha-dependent control of Cryptococcus neoformans in the early phase of pulmonary infection. *PLOS ONE, 9*(1), e87341. doi:10.1371/journal.pone.0087341

Guess, T. E., Rosen, J. A., & McClelland, E. E. (2018). An Overview of Sex Bias in C. neoformans Infections. *J Fungi (Basel), 4*(2). doi:10.3390/jof4020049

Guilliams, M., De Kleer, I., Henri, S., Post, S., Vanhoutte, L., De Prijck, S., . . . Lambrecht, B. N. (2013). Alveolar macrophages develop from fetal monocytes that differentiate into long-lived cells in the first week of life via GM-CSF. *J Exp Med, 210*(10), 1977-1992. doi:10.1084/jem.20131199

Hai, T. P., Van, A. D., Ngan, N. T. T., Nhat, L. T. H., Lan, N. P. H., Vinh Chau, N. V., . . . Day, J. N. (2019). The combination of tamoxifen with amphotericin B, but not with fluconazole, has synergistic activity against the majority of clinical isolates of Cryptococcus neoformans. *Mycoses, 62*(9), 818-825. doi:10.1111/myc.12955

Hansakon, A., Mutthakalin, P., Ngamskulrungroj, P., Chayakulkeeree, M., & Angkasekwinai, P. (2019). Cryptococcus neoformans and Cryptococcus gattii clinical isolates from Thailand display diverse phenotypic interactions with macrophages. *Virulence, 10*(1), 26-36. doi:10.1080/21505594.2018.1556150

Hardison, S. E., Herrera, G., Young, M. L., Hole, C. R., Wozniak, K. L., & Wormley, F. L., Jr. (2012). Protective immunity against pulmonary cryptococcosis is associated with STAT1-mediated classical macrophage activation. *J Immunol, 189*(8), 4060-4068. doi:10.4049/jimmunol.1103455

Hardison, S. E., Ravi, S., Wozniak, K. L., Young, M. L., Olszewski, M. A., & Wormley, F. L., Jr. (2010). Pulmonary infection with an interferon-gamma-producing Cryptococcus neoformans strain results in classical macrophage activation and protection. *Am J Pathol, 176*(2), 774-785. doi:10.2353/ajpath.2010.090634

He, X., Lyons, D. M., Toffaletti, D. L., Wang, F., Qiu, Y., Davis, M. J., . . . Olszewski, M. A. (2012). Virulence factors identified by Cryptococcus neoformans mutant screen differentially modulate lung immune responses and brain dissemination. *Am J Pathol, 181*(4), 1356-1366. doi:10.1016/j.ajpath.2012.06.012

Heiss, C., Klutts, J. S., Wang, Z., Doering, T. L., & Azadi, P. (2009). The structure of Cryptococcus neoformans galactoxylomannan contains beta-D-glucuronic acid. *Carbohydr Res, 344*(7), 915-920. doi:10.1016/j.carres.2009.03.003

Heung, L. J., & Hohl, T. M. (2019). Inflammatory monocytes are detrimental to the host immune response during acute infection with *Cryptococcus neoformans*. *PLOS Pathogens, 15*(3), e1007627. doi:10.1371/journal.ppat.1007627

Hewitt, E. W. (2003). The MHC class I antigen presentation pathway: strategies for viral immune evasion. *Immunology, 110*(2), 163-169. doi:10.1046/j.1365-2567.2003.01738.x

Hey, Y.-Y., Tan, J. K. H., & O'Neill, H. C. (2016). Redefining Myeloid Cell Subsets in Murine Spleen. *Frontiers in Immunology, 6*, 652-652. doi:10.3389/fimmu.2015.00652

Hoeffel, G., Chen, J., Lavin, Y., Low, D., Almeida, F. F., See, P., . . . Ginhoux, F. (2015). C-Myb(+) erythro-myeloid progenitor-derived fetal monocytes give rise to adult tissue-resident macrophages. *Immunity, 42*(4), 665-678. doi:10.1016/j.immuni.2015.03.011

Hoffmann, F. M., Berger, J. L., Lingel, I., Laumonnier, Y., Lewkowich, I. P., Schmudde, I., & König, P. (2018). Distribution and Interaction of Murine Pulmonary Phagocytes in the Naive and Allergic Lung. *Frontiers in immunology, 9*, 1046. doi:10.3389/fimmu.2018.01046

Hole, C. R., Bui, H., Wormley, F. L., & Wozniak, K. L. (2012). Mechanisms of Dendritic Cell Lysosomal Killing of Cryptococcus. *Scientific Reports, 2*(1), 739. doi:10.1038/srep00739

Hole, C. R., Leopold Wager, C. M., Mendiola, A. S., Wozniak, K. L., Campuzano, A., Lin, X., & Wormley, F. L., Jr. (2016). Antifungal activity of plasmacytoid dendritic cells against Cryptococcus neoformans In Vitro requires expression of dectin-3 (CLEC4D) and reactive oxygen species. *Infection and immunity, 84*(9), 2493-2504. doi:10.1128/IAI.00103-16

Huang, L., Nazarova, E. V., & Russell, D. G. (2019). Mycobacterium tuberculosis: Bacterial Fitness within the Host Macrophage. *Microbiol Spectr, 7*(2). doi:10.1128/microbiolspec.BAI-0001-2019

Huang, L., Nazarova, E. V., Tan, S., Liu, Y., & Russell, D. G. (2018). Growth of Mycobacterium tuberculosis in vivo segregates with host macrophage metabolism and ontogeny. *J Exp Med, 215*(4), 1135-1152. doi:10.1084/jem.20172020

Ikeda, R., Shinoda, T., Fukazawa, Y., & Kaufman, L. (1982). Antigenic characterization of Cryptococcus neoformans serotypes and its application to serotyping of clinical isolates. *J Clin Microbiol, 16*(1), 22-29. Retrieved from https://jcm.asm.org/content/jcm/16/1/22.full.pdf

Jamil, K., Polyak, M. J., Feehan, D. D., Surmanowicz, P., Stack, D., Li, S. S., . . . Mody, C. H. (2020). Phagosomal F-Actin Retention by Cryptococcus gattii Induces Dendritic Cell Immunoparalysis. *mBio*, *11*(6), e01821-01820. doi:10.1128/mBio.01821-20

Janout, V., Schell, W. A., Thévenin, D., Yu, Y., Perfect, J. R., & Regen, S. L. (2015). Taming Amphotericin B. *Bioconjugate chemistry*, *26*(10), 2021-2024. doi:10.1021/acs.bioconjchem.5b00463

Jarvis, J. N., Boulle, A., Loyse, A., Bicanic, T., Rebe, K., Williams, A., . . . Meintjes, G. (2009). High ongoing burden of cryptococcal disease in Africa despite antiretroviral roll out. *Aids*, *23*(9), 1182-1183. doi:10.1097/QAD.0b013e32832be0fc

Johnston, S. A., Voelz, K., & May, R. C. (2016). Cryptococcus neoformans Thermotolerance to Avian Body Temperature Is Sufficient For Extracellular Growth But Not Intracellular Survival In Macrophages. *Sci Rep*, *6*, 20977. doi:10.1038/srep20977

Kawakami, K., Kohno, S., Morikawa, N., Kadota, J., Saito, A., & Hara, K. (1994). Activation of macrophages and expansion of specific T lymphocytes in the lungs of mice intratracheally inoculated with Cryptococcus neoformans. *Clinical and Experimental Immunology*, *96*(2), 230-237. Retrieved from https://www.scopus.com/inward/record.uri?eid=2-s2.0-0028301172&partnerID=40&md5=eaeda61d0d2af8c0aa0812e13ff29c8d

Kechichian, T. B., Shea, J., & Del Poeta, M. (2007). Depletion of alveolar macrophages decreases the dissemination of a glucosylceramide-deficient mutant of Cryptococcus neoformans in immunodeficient mice. *Infection and Immunity*, *75*(10), 4792-4798. doi:10.1128/IAI.00587-07

Kohler, J. R., Hube, B., Puccia, R., Casadevall, A., & Perfect, J. R. (2017). Fungi that Infect Humans. *Microbiol Spectr*, *5*(3). doi:10.1128/microbiolspec.FUNK-0014-2016

Kopf, M., Schneider, C., & Nobs, S. P. (2014). The development and function of lung-resident macrophages and dendritic cells. *Nature Immunology*, *16*, 36. doi:10.1038/ni.3052

Kopf, M., Schneider, C., & Nobs, S. P. (2015). The development and function of lung-resident macrophages and dendritic cells. *Nat Immunol*, *16*(1), 36-44. doi:10.1038/ni.3052

Kozel, T. R., & Gotschlich, E. C. (1982). The capsule of cryptococcus neoformans passively inhibits phagocytosis of the yeast by macrophages. *J Immunol*, *129*(4), 1675-1680. Retrieved from https://www.jimmunol.org/content/129/4/1675.long

Kozel, T. R., & Mastroianni, R. P. (1976). Inhibition of phagocytosis by cryptococcal polysaccharide: dissociation of the attachment and ingestion phases of phagocytosis. *Infection and immunity*, *14*(1), 62-67. Retrieved from https://iai.asm.org/content/iai/14/1/62.full.pdf

Kwon-Chung, K. J., & Bennett, J. E. (1984). High prevalence of Cryptococcus neoformans var. gattii in tropical and subtropical regions. *Zentralbl Bakteriol Mikrobiol Hyg A, 257*(2), 213-218.

Kwon-Chung, K. J., Bennett, J. E., Wickes, B. L., Meyer, W., Cuomo, C. A., Wollenburg, K. R., . . . Casadevall, A. (2017). The Case for Adopting the "Species Complex" Nomenclature for the Etiologic Agents of Cryptococcosis. *mSphere, 2*(1). doi:10.1128/mSphere.00357-16

Lam, W. C., Upadhya, R., Specht, C. A., Ragsdale, A. E., Hole, C. R., Levitz, S. M., & Lodge, J. K. (2019). Chitosan Biosynthesis and Virulence in the Human Fungal Pathogen Cryptococcus gattii. *mSphere, 4*(5), e00644-00619. doi:10.1128/mSphere.00644-19

Legrand, P., Romero, E. A., Cohen, B. E., & Bolard, J. (1992). Effects of aggregation and solvent on the toxicity of amphotericin B to human erythrocytes. *Antimicrob Agents Chemother, 36*(11), 2518-2522. doi:10.1128/aac.36.11.2518

Leopold Wager, C. M. (2014). STAT1 signaling is essential for protection against cryptococcus neoformans infection in mice. *The journal of immunology : official journal of the American Association of Immunologists., 193*(8), 4060-4071. doi:10.4049/jimmunol.1400318

Leopold Wager, C. M. (2015). STAT1 signaling within macrophages is required for antifungal activity against Cryptococcus neoformans. *Infection and immunity., 83*(12), 4513-4527. doi:10.1128/IAI.00935-15

Leopold Wager, C. M., Hole, C. R., Campuzano, A., Castro-Lopez, N., Cai, H., Caballero Van Dyke, M. C., . . . Wormley, F. L., Jr. (2018). IFN-γ immune priming of macrophages in vivo induces prolonged STAT1 binding and protection against Cryptococcus neoformans. *PLOS Pathogens, 14*(10). doi:10.1371/journal.ppat.1007358

Leopold Wager, C. M., & Wormley, F. L., Jr. (2014). Classical versus alternative macrophage activation: the Ying and the Yang in host defense against pulmonary fungal infections. *Mucosal Immunol, 7*(5), 1023-1035. doi:10.1038/mi.2014.65

Levitz, S. M., Nong, S.-H., Seetoo, K. F., Harrison, T. S., Speizer, R. A., & Simons, E. R. (1999). Cryptococcus neoformans Resides in an Acidic Phagolysosome of Human Macrophages. *Infection and immunity, 67*(2), 885. Retrieved from http://iai.asm.org/content/67/2/885.abstract

Levitz, S. M., Nong, S. H., Seetoo, K. F., Harrison, T. S., Speizer, R. A., & Simons, E. R. (1999). Cryptococcus neoformans resides in an acidic phagolysosome of human macrophages. *Infection and Immunity, 67*(2), 885-890. Retrieved from https://www.ncbi.nlm.nih.gov/pubmed/9916104

Limper, A. H., Adenis, A., Le, T., & Harrison, T. S. (2017). Fungal infections in HIV/AIDS. *The Lancet Infectious Diseases, 17*(11), e334-e343. doi:https://doi.org/10.1016/S1473-3099(17)30303-1

Lin, K. H., Lin, Y. P., Ho, M. W., Chen, Y. C., & Chung, W. H. (2020). Molecular epidemiology and phylogenetic analyses of environmental and clinical isolates of Cryptococcus gattii sensu lato in Taiwan. *Mycoses, n/a*(n/a). doi:10.1111/myc.13195

Lloyd, C. M., & Marsland, B. J. (2017). Lung Homeostasis: Influence of Age, Microbes, and the Immune System. *Immunity, 46*(4), 549-561. doi:10.1016/j.immuni.2017.04.005

Lopes, J. P., Stylianou, M., Backman, E., Holmberg, S., Ekoff, M., Nilsson, G., & Urban, C. F. (2019). Cryptococcus neoformans Induces MCP-1 Release and Delays the Death of Human Mast Cells. *Frontiers in cellular and infection microbiology, 9*, 289-289. doi:10.3389/fcimb.2019.00289

Ma, H., Croudace, J. E., Lammas, D. A., & May, R. C. (2006). Expulsion of Live Pathogenic Yeast by Macrophages. *Current Biology, 16*(21), 2156-2160. doi:https://doi.org/10.1016/j.cub.2006.09.032

Macura, N., Zhang, T., & Casadevall, A. (2007). Dependence of macrophage phagocytic efficacy on antibody concentration. *Infection and immunity, 75*(4), 1904-1915. doi:10.1128/iai.01258-06

Mansour, M. K., Vyas, J. M., & Levitz, S. M. (2011). Dynamic virulence: real-time assessment of intracellular pathogenesis links Cryptococcus neoformans phenotype with clinical outcome. *mBio, 2*(5). doi:10.1128/mBio.00217-11

Margalit, A., & Kavanagh, K. (2015). The innate immune response to Aspergillus fumigatus at the alveolar surface. *FEMS Microbiol Rev, 39*(5), 670-687. doi:10.1093/femsre/fuv018

Menezes, S., Melandri, D., Anselmi, G., Perchet, T., Loschko, J., Dubrot, J., . . . Guermonprez, P. (2016). The Heterogeneity of Ly6C(hi) Monocytes Controls Their Differentiation into iNOS(+) Macrophages or Monocyte-Derived Dendritic Cells. *Immunity, 45*(6), 1205-1218. doi:10.1016/j.immuni.2016.12.001

Meyer, W., Castañeda, A., Jackson, S., Huynh, M., Castañeda, E., & IberoAmerican Cryptococcal Study, G. (2003). Molecular typing of IberoAmerican Cryptococcus neoformans isolates. *Emerging infectious diseases, 9*(2), 189-195. doi:10.3201/eid0902.020246

Misharin, A. V. (2013). Flow cytometric analysis of macrophages and dendritic cell subsets in the mouse lung. *American journal of respiratory cell and molecular biology., 49*(4), 503-510. doi:10.1165/rcmb.2013-0086MA

Misharin, A. V., Morales-Nebreda, L., Mutlu, G. M., Budinger, G. R. S., & Perlman, H. (2013). Flow cytometric analysis of macrophages and dendritic cell subsets in the mouse lung. *American Journal of Respiratory Cell and Molecular Biology, 49*(4), 503-510. doi:10.1165/rcmb.2013-0086MA

Mitchell, T. G., & Perfect, J. R. (1995). Cryptococcosis in the era of AIDS--100 years after the discovery of Cryptococcus neoformans. *Clinical microbiology reviews, 8*(4), 515-548. Retrieved from https://pubmed.ncbi.nlm.nih.gov/8665468

Molloy, S. F., Kanyama, C., Heyderman, R. S., Loyse, A., Kouanfack, C., Chanda, D., . . . Harrison, T. S. (2018). Antifungal Combinations for Treatment of Cryptococcal Meningitis in Africa. *N Engl J Med, 378*(11), 1004-1017. doi:10.1056/NEJMoa1710922

Monari, C., Bistoni, F., Casadevall, A., Pericolini, E., Pietrella, D., Kozel, T. R., & Vecchiarelli, A. (2005). Glucuronoxylomannan, a microbial compound, regulates expression of costimulatory molecules and production of cytokines in macrophages. *J Infect Dis, 191*(1), 127-137. doi:10.1086/426511

Müller, U., Stenzel, W., Köhler, G., Polte, T., Blessing, M., Mann, A., . . . Alber, G. (2008). A gene-dosage effect for interleukin-4 receptor alpha-chain expression has an impact on Th2-mediated allergic inflammation during bronchopulmonary mycosis. *J Infect Dis, 198*(11), 1714-1721. doi:10.1086/593068

Muller, U., Stenzel, W., Kohler, G., Werner, C., Polte, T., Hansen, G., . . . Alber, G. (2007). IL-13 induces disease-promoting type 2 cytokines, alternatively activated macrophages and allergic inflammation during pulmonary infection of mice with Cryptococcus neoformans. *Journal of immunology (Baltimore, Md. : 1950), 179*(8), 5367-5377. doi:10.4049/jimmunol.179.8.5367

Muntjewerff, E. M., Meesters, L. D., Bogaart, G. v. d., & Revelo, N. H. (2020). Reverse Signaling by MHC-I Molecules in Immune and Non-Immune Cell Types. *Frontiers in immunology, 11*(3264). doi:10.3389/fimmu.2020.605958

Murray, P. J. (2018). Immune regulation by monocytes. *Seminars in Immunology, 35*, 12-18. doi:https://doi.org/10.1016/j.smim.2017.12.005

Nelson, B. N., Hawkins, A. N., & Wozniak, K. L. (2020). Pulmonary Macrophage and Dendritic Cell Responses to Cryptococcus neoformans. *Frontiers in cellular and infection microbiology, 10*, 37-37. doi:10.3389/fcimb.2020.00037

Odds, F. C., Brown, A. J., & Gow, N. A. (2003). Antifungal agents: mechanisms of action. *Trends Microbiol, 11*(6), 272-279. doi:10.1016/s0966-842x(03)00117-3

Olszewski, M. A., Zhang, Y., & Huffnagle, G. B. (2010). Mechanisms of cryptococcal virulence and persistence. *Future Microbiol, 5*(8), 1269-1288. doi:10.2217/fmb.10.93

Osterholzer, J. J., Chen, G. H., Olszewski, M. A., Curtis, J. L., Huffnagle, G. B., & Toews, G. B. (2009). Accumulation of CD11b+ lung dendritic cells in response to fungal infection results from the CCR2-mediated recruitment and differentiation of Ly-6Chigh monocytes. *Journal of immunology, 183*(12), 8044-8053. doi:10.4049/jimmunol.0902823

Osterholzer, J. J., Chen, G. H., Olszewski, M. A., Zhang, Y. M., Curtis, J. L., Huffnagle, G. B., & Toews, G. B. (2011). Chemokine receptor 2-mediated accumulation of fungicidal exudate macrophages in mice that clear cryptococcal lung infection. *American Journal of Pathology, 178*(1), 198-211. doi:10.1016/j.ajpath.2010.11.006

Osterholzer, J. J., Curtis, J. L., Polak, T., Ames, T., Chen, G. H., McDonald, R., . . . Toews, G. B. (2008). CCR2 mediates conventional dendritic cell recruitment and the formation of bronchovascular mononuclear cell infiltrates in the lungs of mice infected with cryptococcus neoformans. *Journal of Immunology, 181*(1), 610-620. doi:10.4049/jimmunol.181.1.610

Osterholzer, J. J., Milam, J. E., Chen, G. H., Toews, G. B., Huffnagle, G. B., & Olszewski, M. A. (2009). Role of dendritic cells and alveolar macrophages in regulating early host defense against pulmonary infection with Cryptococcus neoformans. *Infection and Immunity, 77*(9), 3749-3755. doi:10.1128/IAI.00454-09

Osterholzer, J. J., Surana, R., Milam, J. E., Montano, G. T., Chen, G. H., Sonstein, J., . . . Olszewski, M. A. (2009). Cryptococcal urease promotes the accumulation of immature dendritic cells and a non-protective T2 immune response within the lung. *Am J Pathol, 174*(3), 932-943. doi:10.2353/ajpath.2009.080673

Park, B. J., Wannemuehler, K. A., Marston, B. J., Govender, N., Pappas, P. G., & Chiller, T. M. (2009). Estimation of the current global burden of cryptococcal meningitis among persons living with HIV/AIDS. *Aids, 23*(4), 525-530. doi:10.1097/QAD.0b013e328322ffac

Park, B. J., Wannemuehler, K. A., Marston, B. J., Govender, N., Pappas, P. G., & Chiller, T. M. (2009). Estimation of the current global burden of cryptococcal meningitis among persons living with HIV/AIDS. *Aids, 23*(4), 525-530. doi:10.1097/QAD.0b013e328322ffac

Peng, C. A., Gaertner, A. A. E., Henriquez, S. A., Fang, D., Colon-Reyes, R. J., Brumaghim, J. L., & Kozubowski, L. (2018). Fluconazole induces ROS in Cryptococcus neoformans and contributes to DNA damage in vitro. *PLOS ONE, 13*(12), e0208471-e0208471. doi:10.1371/journal.pone.0208471

Pericolini, E., Cenci, E., Monari, C., De Jesus, M., Bistoni, F., Casadevall, A., & Vecchiarelli, A. (2006). Cryptococcus neoformans capsular polysaccharide component galactoxylomannan induces apoptosis of human T-cells through activation of caspase-8. *Cell Microbiol, 8*(2), 267-275. doi:10.1111/j.1462-5822.2005.00619.x

Piccioni, M., Monari, C., Bevilacqua, S., Perito, S., Bistoni, F., Kozel, T. R., & Vecchiarelli, A. (2011). A critical role for FcgammaRIIB in up-regulation of Fas ligand induced by a microbial polysaccharide. *Clin Exp Immunol, 165*(2), 190-201. doi:10.1111/j.1365-2249.2011.04415.x

Pirofski, L.-a., & Casadevall, A. (2020). The state of latency in microbial pathogenesis. *The Journal of Clinical Investigation, 130*(9), 4525-4531. doi:10.1172/JCI136221

Pisu, D., Huang, L., Grenier, J. K., & Russell, D. G. (2020). Dual RNA-Seq of Mtb-Infected Macrophages In Vivo Reveals Ontologically Distinct Host-Pathogen Interactions. *Cell Rep, 30*(2), 335-350.e334. doi:10.1016/j.celrep.2019.12.033

Rajasingham, R., Smith, R. M., Park, B. J., Jarvis, J. N., Govender, N. P., Chiller, T. M., . . . Boulware, D. R. (2017). Global burden of disease of HIV-associated cryptococcal meningitis: an updated analysis. *The Lancet. Infectious diseases, 17*(8), 873-881. doi:10.1016/S1473-3099(17)30243-8

Ramachandran, P., Pellicoro, A., Vernon, M. A., Boulter, L., Aucott, R. L., Ali, A., . . . Iredale, J. P. (2012). Differential Ly-6C expression identifies the recruited macrophage phenotype, which orchestrates the regression of murine liver fibrosis. *Proceedings of the National Academy of Sciences, 109*(46), E3186-E3195. doi:10.1073/pnas.1119964109

Sabiiti, W., Robertson, E., Beale, M. A., Johnston, S. A., Brouwer, A. E., Loyse, A., . . . Bicanic, T. (2014). Efficient phagocytosis and laccase activity affect the outcome of HIV-associated cryptococcosis. *J Clin Invest, 124*(5), 2000-2008. doi:10.1172/jci72950

Santangelo, R., Zoellner, H., Sorrell, T., Wilson, C., Donald, C., Djordjevic, J., . . . Wright, L. (2004). Role of extracellular phospholipases and mononuclear phagocytes in dissemination of cryptococcosis in a murine model. *Infect Immun, 72*(4), 2229-2239. doi:10.1128/iai.72.4.2229-2239.2004

Serbina, N. V., Jia, T., Hohl, T. M., & Pamer, E. G. (2008). Monocyte-mediated defense against microbial pathogens. *Annual review of immunology, 26*, 421-452. doi:10.1146/annurev.immunol.26.021607.090326

Shao, X., Mednick, A., Alvarez, M., Van Rooijen, N., Casadevall, A., & Goldman, D. L. (2005). An innate immune system cell is a major determinant of species-related susceptibility differences to fungal pneumonia. *Journal of Immunology, 175*(5), 3244-3251. doi:10.4049/jimmunol.175.5.3244

Shortman, K., & Liu, Y. J. (2002). Mouse and human dendritic cell subtypes. *Nat Rev Immunol, 2*(3), 151-161. doi:10.1038/nri746

Sloan, D. J., & Parris, V. (2014). Cryptococcal meningitis: epidemiology and therapeutic options. *Clinical epidemiology, 6*, 169-182. doi:10.2147/CLEP.S38850

Smith, L. M., Dixon, E. F., & May, R. C. (2015). The fungal pathogen Cryptococcus neoformans manipulates macrophage phagosome maturation. *Cell Microbiol, 17*(5), 702-713. doi:10.1111/cmi.12394

Stepanova, A., Vasilyeva, N., Yamaguchi, M., Chibana, H., Bosak, I., & Filippova, L. (2018). Ultrastructural patterns of interactions between murine lung macrophages and yeast cells of cryptococcus neoformans strains with different virulence. *Medical Mycology Journal, 59*(1), E1-E6. doi:10.3314/mmj.16-00009

Subramani, A., Griggs, P., Frantzen, N., Mendez, J., Tucker, J., Murriel, J., . . . Nelson, D. E. (2020). Intracellular Cryptococcus neoformans disrupts the transcriptome profile of M1- and M2-polarized host macrophages. *PLoS One, 15*(8), e0233818-e0233818. doi:10.1371/journal.pone.0233818

Sung, S.-S. J., Fu, S. M., Rose, C. E., Gaskin, F., Ju, S.-T., & Beaty, S. R. (2006). A Major Lung CD103 (α_E)-β₇ Integrin-Positive Epithelial Dendritic Cell Population Expressing Langerin and Tight Junction Proteins. *The Journal of Immunology, 176*(4), 2161-2172. doi:10.4049/jimmunol.176.4.2161

Tan, S. Y., & Krasnow, M. A. (2016). Developmental origin of lung macrophage diversity. *Development, 143*(8), 1318-1327. doi:10.1242/dev.129122

Tenor, J. L., Oehlers, S. H., Yang, J. L., Tobin, D. M., & Perfect, J. R. (2015). Live Imaging of Host-Parasite Interactions in a Zebrafish Infection Model Reveals Cryptococcal Determinants of Virulence and Central Nervous System Invasion. *mBio, 6*(5), e01425-01415. doi:10.1128/mBio.01425-15

Todd, E. M., Zhou, J. Y., Szasz, T. P., Deady, L. E., D'Angelo, J. A., Cheung, M. D., . . . Morley, S. C. (2016). Alveolar macrophage development in mice requires L-plastin for cellular localization in alveoli. *Blood, 128*(24), 2785-2796. doi:10.1182/blood-2016-03-705962

Traynor, T. R., Kuziel, W. A., Toews, G. B., & Huffnagle, G. B. (2000). CCR2 Expression Determines T1 Versus T2 Polarization During Pulmonary *Cryptococcus neoformans* Infection. *J Immunol, 164*(4), 2021-2027. Retrieved from http://www.jimmunol.org/cgi/content/abstract/164/4/2021

Vecchiarelli, A., Pietrella, D., Bistoni, F., Kozel, T. R., & Casadevall, A. (2002). Antibody to Cryptococcus neoformans capsular glucuronoxylomannan promotes expression of interleukin-12Rbeta2 subunit on human T cells in vitro through effects mediated by antigen-presenting cells. *Immunology, 106*(2), 267-272. doi:10.1046/j.1365-2567.2002.01419.x

Vermaelen, K., & Pauwels, R. (2004). Accurate and simple discrimination of mouse pulmonary dendritic cell and macrophage populations by flow cytometry: Methodology and new insights. *Cytometry Part A, 61*(2), 170-177. doi:10.1002/cyto.a.20064

Voelz, K., Lammas, D. A., & May, R. C. (2009). Cytokine signaling regulates the outcome of intracellular macrophage parasitism by Cryptococcus neoformans. *Infection and immunity, 77*(8), 3450-3457. doi:10.1128/iai.00297-09

Wang, Y., Aisen, P., & Casadevall, A. (1995). Cryptococcus neoformans melanin and virulence: mechanism of action. *Infection and immunity, 63*(8), 3131-3136. doi:10.1128/IAI.63.8.3131-3136.1995

Wieczorek, M., Abualrous, E. T., Sticht, J., Álvaro-Benito, M., Stolzenberg, S., Noé, F., & Freund, C. (2017). Major Histocompatibility Complex (MHC) Class I and MHC Class II Proteins: Conformational Plasticity in Antigen Presentation. *Frontiers in immunology, 8*, 292-292. doi:10.3389/fimmu.2017.00292

Wozniak, K. L. (2018). Interactions of Cryptococcus with Dendritic Cells. *J Fungi (Basel), 4*(1). doi:10.3390/jof4010036

Wozniak, K. L., Ravi, S., Macias, S., Young, M. L., Olszewski, M. A., Steele, C., & Wormley, F. L. (2009). Insights into the mechanisms of protective immunity against *Cryptococcus neoformans* infection using a mouse model of pulmonary cryptococcosis. *PLoS One, 4*(9), e6854. doi:10.1371/journal.pone.0006854

Wozniak, K. L., Vyas, J. M., & Levitz, S. M. (2006). In vivo role of dendritic cells in a murine model of pulmonary cryptococcosis. *Infection and Immunity, 74*(7), 3817-3824. doi:10.1128/IAI.00317-06

Xu, S., & Shinohara, M. L. (2017). Tissue-resident macrophages in fungal infections. *Frontiers in Immunology, 8*(DEC). doi:10.3389/fimmu.2017.01798

Yang, J., Zhang, L., Yu, C., Yang, X.-F., & Wang, H. (2014). Monocyte and macrophage differentiation: circulation inflammatory monocyte as biomarker for inflammatory diseases. *Biomarker research, 2*(1), 1-1. doi:10.1186/2050-7771-2-1

Zaragoza, O. (2019). Basic principles of the virulence of Cryptococcus. *Virulence, 10*(1), 490-501. doi:10.1080/21505594.2019.1614383

Zaragoza, O., Chrisman, C. J., Castelli, M. V., Frases, S., Cuenca-Estrella, M., Rodríguez-Tudela, J. L., & Casadevall, A. (2008). Capsule enlargement in Cryptococcus neoformans confers resistance to oxidative stress suggesting a mechanism for intracellular survival. *Cell Microbiol, 10*(10), 2043-2057. doi:10.1111/j.1462-5822.2008.01186.x

Zaynagetdinov, R., Sherrill, T. P., Kendall, P. L., Segal, B. H., Weller, K. P., Tighe, R. M., & Blackwell, T. S. (2013). Identification of myeloid cell subsets in murine lungs using flow cytometry. *American Journal of Respiratory Cell and Molecular Biology, 49*(2), 180-189. doi:10.1165/rcmb.2012-0366MA

Zhang, C., Yang, M., & Ericsson, A. C. (2021). Function of Macrophages in Disease: Current Understanding on Molecular Mechanisms. *Frontiers in immunology, 12*, 620510-620510. doi:10.3389/fimmu.2021.620510

Zhang, Y., Wang, F., Bhan, U., Huffnagle, G. B., Toews, G. B., Standiford, T. J., & Olszewski, M. A. (2010). TLR9 signaling is required for generation of the adaptive immune protection in Cryptococcus neoformans-infected lungs. *Am J Pathol, 177*(2), 754-765. doi:10.2353/ajpath.2010.091104

Zhang, Y., Wang, F., Tompkins, K. C., McNamara, A., Jain, A. V., Moore, B. B., . . . Olszewski, M. A. (2009). Robust Th1 and Th17 immunity supports pulmonary clearance but cannot prevent systemic dissemination of highly virulent Cryptococcus neoformans H99. *Am J Pathol, 175*(6), 2489-2500. doi:10.2353/ajpath.2009.09053

VITA

Ashlee Hawkins

Candidate for the Degree of

Master of Science

Thesis: AN ANALYSIS OF THE INTERACTIONS BETWEEN CRYPTOCOCCUS NEOFORMANS AND MURINE PULMONARY PHAGOCYTE SUBSETS

Major Field: Microbiology

Biographical:

Education:

Completed the requirements for the Master of Science in Microbiology at Oklahoma State University, Stillwater, Oklahoma in May, 2021.

Completed the requirements for the Bachelor of Science Microbiology at Oklahoma State University, Stillwater, Oklahoma in 2018.

Leadership:

Black Graduate Student Association
President: Fall 2019 - Spring 2020
Secretary: Fall 2018 - Spring 2019

Microbiology and Molecular Genetics Graduate Student Association
President: Fall 2020 - Spring 2021
Treasurer: Fall 2019 - Spring 2020

Graduate Research Assistant
Wozniak Lab: Fall 2018 - Spring 2021